

Phase change-related thermal property characterization and enhancement in carbon-based organic phase change composites

Cite as: Appl. Phys. Rev. **11**, 021322 (2024); doi: [10.1063/5.0165697](https://doi.org/10.1063/5.0165697)

Submitted: 29 June 2023 · Accepted: 16 April 2024 ·

Published Online: 23 May 2024 · Publisher error corrected: 30 May 2024



Mingxin Li,¹ Xuanjie Wang,¹ Junhua Shen,² Dong Zhao,¹ and Jie Lian^{1,2,a)}

AFFILIATIONS

¹Department of Mechanical, Aerospace, and Nuclear Engineering, Rensselaer Polytechnic Institute, 110, 8th Street, Troy, New York 12180, USA

²Department of Materials Science and Engineering, Rensselaer Polytechnic Institute, 110, 8th Street, Troy, New York 12180, USA

Note: This paper is part of the APR Special Topic on New Carbon Materials.

^{a)}Author to whom correspondence should be addressed: lianj@rpi.edu

ABSTRACT

By utilizing the significant amount of energy absorbed and released during their phase transitions, phase change materials (PCMs) can capture and store thermal energy to fill gaps between supply and demand. Due to their many favorable properties, organic PCMs have gained attention in a wide range of applications. Nevertheless, their inherent low thermal conductivity has limited the direct use of organic PCMs in thermal energy storage (TES). Extensive research has been conducted on enhancing organic PCM thermal conductivity by incorporating high thermal conductivity materials. Owing to their high thermal conductivity and low density, carbon-based materials have been extensively used for thermal conductivity enhancement in phase change composites (PCCs). Carbon-based organic PCCs, which incorporate highly thermally conductive carbon allotropes and their direct chemical derivatives with organic PCMs, are a group of diverse PCCs with highly promising potential for TES applications. Adequate latent heat and shape stability performances are crucial to the success of the applicational performances of these PCCs. Much empirical research has pushed efforts to enhance these phase change properties, yet a logical understanding of these enhancement efforts based on the thermodynamics and intermolecular interactions of carbon-based organic PCCs has been elusive. In particular, the effect of characterization methods on the evaluation of phase change properties has been largely understudied. This review strives to provide novel physical and chemical insights into latent heat and shape stabilization evaluation processes and enhancement efforts in carbon-based organic PCCs through a detailed review and analysis of recent literature. The review provides an unprecedented comprehension of newly developed PCCs that challenge the traditional understanding that the latent heat of PCCs cannot exceed that of its base PCM. Efforts on phase change property enhancement driven by these new insights have the potential for carbon-based organic PCCs to succeed in a variety of TES applications, including solar-thermal harvesting, thermal management of batteries and electronics, thermoregulating textiles, and infrared stealth and infrared responsive materials.

Published under an exclusive license by AIP Publishing. <https://doi.org/10.1063/5.0165697>

TABLE OF CONTENTS

I. INTRODUCTION.....	2	III. ORGANIC PHASE CHANGE MATERIALS AND THEIR CARBON-BASED COMPOSITES	6
II. LATENT HEAT AND ITS CHARACTERIZATION IN CARBON-BASED PHASE CHANGE COMPOSITES	3	IV. LATENT HEAT ENHANCEMENT	8
A. Thermodynamics of phase transition in solids and liquids	3	A. Enhanced crystallization.....	9
B. Calorimetric characterization methods.....	5	B. Compressive stress.....	10
1. Differential scanning calorimetry.....	5	C. Intermolecular attraction	11
2. T-history method	5	D. Hydrogen bonding	12
V. SHAPE STABILITY ENHANCEMENT.....	12	A. Microencapsulation.....	12

B. Nano-material incorporation	14
C. Porous material stabilization	16
VI. APPLICATIONS OF SHAPE-STABLE CARBON-BASED ORGANIC PHASE CHANGE COMPOSITES WITH HIGH LATENT HEAT	17
A. Solar-thermal energy conversion and storage.....	17
B. Thermal management of batteries and electronic devices	17
C. Thermoregulating textiles.....	18
D. Infrared-stealth and infrared-responsive materials	19
VII. SUMMARY AND OUTLOOK.....	21

I. INTRODUCTION

Momentously transformed by the continuous rapid increase in energy consumption in the past seven decades, our global economy is experiencing unprecedented prosperity. However, this prosperity, mainly built through the consumption of fossil fuels, has caused a wide range of environmental and societal issues. Demands for sustainable development have led to extensive research in renewable energy sources and energy conservation methods. Most energy loss is through thermal dissipation, so how to reduce heat dissipation and effectively use heat dissipation is of great significance to renewable energy.¹ Thermal energy storage (TES) technologies accumulate otherwise dissipated thermal energy in useful quantities for a wide range of applications.²

PCMs have seen wide TES-based applications by storing and releasing large quantities of thermal energy as latent heat during their phase change processes, including solar-thermal energy harvesting, battery temperature management, textile thermoregulation, etc.^{3,4} As the successors of first-generation inorganic PCMs, second-generation organic PCMs possess many favorable attributes, including low cost, low density, minimal supercooling, no phase separation, good biocompatibility, good chemical stability, high latent heat, moderate phase change temperature, and, therefore, the most common types of PCMs currently used for applications.^{5–7} However, the thermal performance of common organic PCMs, including paraffin, fatty alcohols, fatty acids, and polyethylene glycols (PEGs), is inherently limited by their low thermal conductivity and tendency to lose shape stability after the solid-liquid phase change.^{8,9} To overcome these shortcomings, organic PCMs are often incorporated with highly thermally conductive carbon materials to form PCCs with better overall heat utilization and enhanced energy storage and release rates.¹⁰ Carbon allotropes, including carbon nanotubes (CNTs), graphene, graphite, carbon black, and their multiscale derivatives, are commonly referred to as carbon materials. Due to their high thermal conductivity, low density, good wettability, tunable functional surface, and high absorption rate of visible solar radiation, they are highly suitable for compositing with PCMs to achieve enhanced thermal conductivity and gain useful functional properties.^{3,11–13} From the large variety of functional carbon materials available today, an equal, if not larger, group of carbon-based organic PCCs has been developed and reported with enhanced thermal conductivity.¹⁴ However, existing research on carbon-based organic PCCs often overlooks their phase change-related thermal performances, including latent heat, phase change temperature, and thermal and shape stability of these PCCs.¹⁵ Latent heat of PCCs determines their energy storage capacity, which, for TES purpose, is an equally if not

even more critical factor in determining the applicational value of particular PCCs compared to their thermal conductivity.

Abundant methods have been developed for characterizing the latent heat of PCCs, accommodating different sample sizes with varying measurement accuracies. However, the research on calorimetric characterization methods has not been well-established as on thermal conductivity characterization methods. Studies on the effects of differential scanning calorimetry (DSC) and the t-history methods on the measured latent heat values of carbon-based organic PCCs are relatively new and inconclusive. The study on latent heat enhancement of PCCs, particularly carbon-based organic PCCs, is even newer. With the possibility of latent heat enhancement by forming composites of organic PCMs with carbon-based materials only recognized in the late 2000s and groundbreaking yet limited research gaining attention in the 2010s and early 2020s, no systematic studies have been conducted to elucidate the underlying mechanism in latent heat enhancements.

Traditionally, it has been accepted that compositing PCMs with non-phase-changing materials will decrease latent heat, and a trade-off in latent heat is inevitable when attempting to increase the thermal conductivity of PCCs.¹⁵ However, with an increased effort on research in novel carbon-based organic PCCs, it has been gradually confirmed that the non-phase-changing carbon-based materials affect the overall physical properties of the PCCs much more than providing a thermal percolation path.¹⁶ Interactions between the PCM and carbon-based materials are multiscale and complex. Intermolecular interactions such as C-H···π bonds and hydrogen bonds may occur between certain PCMs and carbon-based materials.^{17–21} Graphene-based materials in PCCs may influence the crystallization of certain PCMs.²² Macroscale carbon-based materials may also apply compressive stress to the PCM during its solid–liquid phase change.²³ Under certain circumstances, all of these factors (see Fig. 1) may lead the latent heat of PCCs to

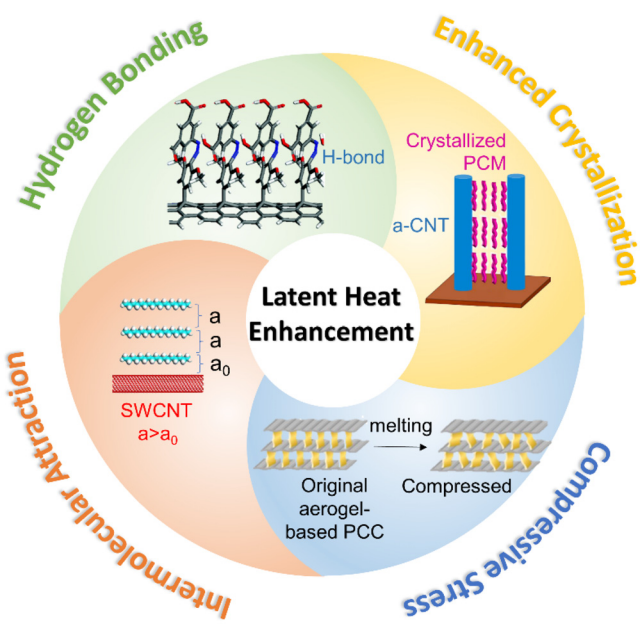


FIG. 1. Schematic of latent heat enhancement mechanisms of carbon-based organic PCCs.

exceed that of pure PCMs. Although it is generally accepted that the interactions between the carbon-based material and the organic PCM can enhance the latent heat of PCCs, there is no consensus on what types of interactions will guarantee this enhancement. Several proposed interaction mechanisms that result in enhanced latent heat remain contentious.²⁴

In addition to their latent heat, the interaction between carbon-based materials and PCMs in PCCs can also significantly impact the shape stability of PCCs.³ Defined as the ability to withstand leakage and retain their shape in the solid state during phase transition, the shape stability of PCCs is vital to their practical application and prolonged usage.²⁵ Carbon-based materials can improve the shape stability of PCCs in a multitude of manners.²⁶ CNTs and carbon nanospheres encapsulate PCMs on nano- and micro-levels to achieve shape stability.^{27–30} The surface properties and interlayer distance between 2D graphene-based nano-materials are tunable.³ Therefore, various interfacial interactions between them and PCMs are also widely used to shape stabilize PCCs. However, the most extensive shape-stabilizing technique of PCCs is undeniably the incorporation of PCMs in porous carbon-based 3D macrostructures. Either assembled bottom-up from 1D or 2D carbon nano-materials or fabricated from the carbonization of bulk polymeric or bio-based materials, PCMs can be impregnated into a porous carbon-based macrostructure in its liquid state and solidified into a PCC. Capillary force, surface tension, hydrogen bonding, Van der Waal's force, or a combination of several factors allow these porous carbon-based macrostructures to hold the PCMs in their pores.²⁵ The characterization of shape stability in PCCs is commonly conducted by simply placing a piece of PCC on top of a filter paper on a hot plate heated to or above the solid-liquid phase transition temperature. Leakage of the PCC is evaluated by whether a PCM exudation blot appears on the filter paper and to what extent.³¹ Thermomechanical and compression testing are also common tests conducted on PCCs to evaluate their shape stability alongside leakage testing.³

In recent years, carbon-based organic PCCs have largely proven to outperform inorganic PCMs and pure organic PCMs in a range of TES applications, including thermal management in batteries, consumer electronics, textiles, and solar-thermal harvesting and storage devices, thanks to their favorable phase transition temperature range and enhanced thermal conductivity.^{3,32} Early commercialization of these carbon-based organic PCCs has demanded more improvements to their overall economic performance and durability.^{33,34} These performance criteria are closely linked to the phase change properties of PCCs.³⁵ PCCs with increased latent heat and shape stability are rapidly gaining favorability in real-life applications where total energy storage capacity and an extended lifespan are essential.^{36,37}

In this review, we present a comprehensive study on phase change-related thermal properties of carbon-based organic PCCs, including latent heat and shape stability, which are arguably the most important phase change-related properties of PCCs relating to TES applications. The research progress on enhancing latent heat and shape stability is emphasized. First, we introduced the concept of latent heat and presented the thermodynamics involved in its theoretical understanding. The influence of common calorimetric methods such as DSC and the t-history method on latent heat measurement is then elaborated to elucidate any experimental-based bias involved in evaluating latent heat of carbon-based organic PCCs. Then, we presented

the newly developed methods for enhancing latent heat in carbon-based organic PCCs, particularly those fascinating approaches where the latent heat of the PCC can exceed that of the pure PCM. Next, we summarized innovative shape-stabilizing methods of carbon-based organic PCC and how well these methods prevent leakage at temperatures above the PCC's phase transition point. Finally, we reviewed how the enhancement of phase change properties, with latent heat and shape stability in particular, has impacted TES and other relevant industries. New advancements in enhancing phase change properties and their applications in the near future are also discussed.

II. LATENT HEAT AND ITS CHARACTERIZATION IN CARBON-BASED PHASE CHANGE COMPOSITES

Thermal energy is stored in matter in three forms: latent heat, sensible heat, and thermochemical heat.^{38,39} The heat absorbed and released by the matter at a constant temperature T_{pc} during phase transition is the latent heat $\Delta_{pc}h$, also called phase change enthalpy, as it is equivalent to the enthalpy change during phase change. PCMs can store significant amounts of latent heat during their phase transition process.^{40,41} It is usually a magnitude larger than the sensible heat stored in the same mass.^{42,43} The utilization of energy stored in latent heat is also much more easily accessible than that stored in thermochemical heat.⁴⁴ Compared to solid-solid transitions, solid-liquid transitions have higher latent heat, while compared to solid-gas and liquid-gas phase transitions, volume change in PCMs during solid-liquid transitions is small.^{45,46} Therefore, most PCMs and PCCs, including almost all carbon-based PCCs, utilize latent heat absorbed and released during solid-liquid phase transitions. Ultimately, utilizing the functional properties of non-phase changing components to promote accessible and effective use of latent heat from PCM solid-liquid phase transitions is the primary purpose of compositing PCMs with materials such as carbon allotropes and their derivatives, including CNTs, graphene, and graphene oxide (GO).

A. Thermodynamics of phase transition in solids and liquids

Solid-liquid and liquid-solid phase transitions in the form of melting and solidification are the most common forms of phase transition utilized by carbon-based organic PCCs. The thermodynamic properties of the PCC during melting and solidification, such as latent heat and phase transition temperature, are some of the most important criteria in evaluating their performance.

Arguably, the most important thermodynamic criterion for evaluating the usefulness of a particular PCM or PCC for thermal energy storage is the latent heat absorbed during the solid-liquid transition, commonly called the latent heat of fusion L_f . If we define the melting temperature as T_m , the change in the volume of the PCM or PCC as ΔV , and the pressure-temperature derivative of the PCM or PCC as dp/dT , the latent heat of fusion can be theoretically determined by the Clapeyron equation,^{47,48}

$$L_f = T_m \frac{dp}{dT} \Big|_{T=T_m} \Delta V. \quad (1)$$

Despite the difficulty in determining the pressure change at the melting temperature, the Clapeyron equation provides an intuitive guideline for designing PCCs with higher latent heat, such as carbon-based PCCs.⁴⁸

Compared to the macroscopic perspective of the Clapeyron equation, a microscopic approach can also be used to analyze the thermodynamic properties of the solid–liquid and liquid–solid phase transitions. If we take the solidification process as an example, the intermolecular forces at the solidification temperature are the driving cause for disorder molecules to form a periodic structure. Phase change-related quantities, such as the latent heat and phase transition temperature, are a function of these intermolecular forces. The microscopic non-bonding forces that act on two molecules at sites i and j can be described analytically by the sum of the Lennard-Jones and Coulomb potentials $V(r_{ij})$,^{49,50}

$$V(r_{ij}) = 4\epsilon_{ij} \left[\left(\frac{\sigma_{ij}}{r_{ij}} \right)^{12} - \left(\frac{\sigma_{ij}}{r_{ij}} \right)^6 \right] + \frac{kq_i q_j}{r_{ij}}, \quad (2)$$

where r_{ij} is the distance between the two molecules, ϵ_{ij} is the depth of the potential well, and σ_{ij} is the distance at which the Lennard-Jones potential energy is 0, k is the Coulomb constant, and q_i and q_j are the charges of the two molecules. At the small distances between adjacent molecules, r_{ij} approaches 0. Therefore, the microscopic non-binding forces follow the trend of the exponents in the terms in Eq. (2), resulting in the repulsive force with an exponent of 12 being much more substantial than the attractive force with an exponent of 6 and the Coulomb electrostatic force with an exponent of 1. In a system with more than two molecules, multibody terms need to be added to Eq. (2); however, the repulsive force dominates at small distances. Therefore, the repulsive force becomes the dominate force in arranging the configuration and orientation of the molecules when forming the periodic microstructure. The presence of repulsive forces between molecules during solidification hinders the attempt to form a solid structure with periodic microstructures and, therefore, can increase the latent heat of solidification and decrease the solidification temperature.^{47,48,51} What microstructures are created by these microscopic forces directly determines at what temperature solidification will occur and how large the latent heat will be. With a good understanding of the importance of microscopic forces to the latent heat and phase change temperatures, surfactants can be added to prevent the amalgamation of carbon additives in PCCs and aggravate the impact of the microscopic forces exerted by the carbon additives onto the PCM matrix.⁵²

The effect of the microscopic forces on the latent heat and phase transition temperatures of the PCMs and PCCs can also be studied by analyzing the interfacial energy between the solid and liquid phases. The interfacial energy approach has proven especially useful for studying the Gibbs–Thomson effect, which tributes the change in the enthalpy of the phase change material to the surface curvature of the interface.⁴⁷

The decreased melting temperature of PCMs with a small spherical crystal radius of r can be described by the Gibbs–Thomson equation shown in the following:^{53,54}

$$T_m(r) = T_m(\infty) - \frac{2T_m(\infty)\sigma_{sl}}{\Delta H_f(\infty)\rho_s r} \quad (3)$$

where $T_m(\infty)$, $\Delta H_f(\infty)$, and ρ_s are the bulk melting temperature, the bulk latent heat of fusion, and the bulk solid density, respectively. σ_{sl} is the solid–liquid interfacial energy. The decrease in melting temperature of the small spherical crystal compared to the bulk PCM is

inversely linear to the particle size of the PCM. The Gibb–Thompson equation applies to PCCs formed by confined organic PCMs in CNTs.²⁷ The Gibbs–Thomson equation can also derive a size-dependent latent heat of fusion $\Delta H_f(r)$,^{53,55}

$$\Delta H_f(r) = \Delta H_f(\infty) - \frac{2\sigma_{sl}}{\rho_s r}. \quad (4)$$

When the potential energy of the organic PCM–carbon interface has a lower potential energy compared to the bulk PCM, the solid–liquid interfacial energy σ_{sl} becomes negative, therefore allowing $\Delta H_f(r)$ of the composite to be greater than $\Delta H_f(\infty)$. For analyzing the melting temperature and latent heat of fusion of PCC with more complex microstructures, Eq. (4) cannot be directly used. However, as will be further discussed in Sec. IV, interfacial potential energy plays an indispensable role in the change in melting temperature and latent heat of fusion of PCCs compared to pure PCMs. A variety of shifts in microstructure at the interface, such as changes in molecular distances or the molecular configuration of PCM molecules, will significantly impact how the latent heat values of PCCs as compared to that of its pure PCM components.

The thermodynamic investigation of PCMs often assumes ideal PCMs with the same solidification and melting temperatures and the same latent heat of solidification and fusion. However, in the case of a realistic PCM or PCC with solid–liquid phase transition, the phase change process is often not ideal and occurs in a narrow temperature range ΔT_{pc} . Often, the solidification temperature is slightly lower than the melting temperature, in a phenomenon called supercooling.⁵⁶ During the supercooling, due to the metastable cool liquid PCM, crystallization does not occur until a nucleation temperature T_n is achieved.⁵⁷ As a result of supercooling, hysteresis is observed in the temperature-to-enthalpy plot of a PCM during the solid–liquid phase transition. The difference between the theoretical melting temperature and the nucleation temperature T_n is the degree of supercooling.⁵⁸ A significant degree of supercooling is generally not desired as it prevents latent heat release at the desired applicational temperature and increases the energy consumption needed to release latent heat.⁵⁸ Multiple approaches can be taken to decrease the degree of supercooling, including increasing the volume of the liquid PCM,⁵⁹ decreasing the cooling rate,⁶⁰ increasing the roughness of the liquid PCM's container,⁶¹ and adding nucleation agents, such as carbon-based additives.^{62,63}

In addition to phase transition temperatures and latent heat, thermal conductivity is also an important criterion for assessing the performance of PCMs and PCCs for thermal energy storage. High thermal conductivity is desired for PCMs and PCCs in their solid state before melting to improve their thermal response rate and thermal storage efficiency. In recent years, owing to the development of several innovative material designs and PCC fabrication techniques, this type of thermal conductivity has significantly improved in carbon-based organic PCCs.^{3,14,64} However, since the thermal conductivity of PCMs and PCCs before melting and solidification is independent of the phase transition process,⁶⁵ this review does not discuss the details of the materials science involved in pre-phase transition thermal conductivity.

Unlike the predominantly temperature-independent thermal conductivity of the PCMs and PCCs in the solid and liquid phases before melting and solidification, the thermal conductivity of carbon-based

organic PCCs exhibits a significant increase when the temperature rises to near the melting point and experiences a sharp drop to levels lower than the thermal conductivity in the solid state when the PCM matrix completely liquifies.^{65,66} The thermal conductivity increase immediately before melting has been hypothetically attributed to the accelerated molecular vibration in the ordered microstructure of the PCM matrix, while the sharp decrease immediately after complete melting is attributed to the microstructure of the PCM matrix transforming from an orderly structure in the solid state into a disorderly structure in the liquid state.⁶⁵ Up to now, experimental and simulation efforts have yet to be made to validate these hypotheses.

B. Calorimetric characterization methods

The heat flow into and out of a sample as a function of temperature is determined by calorimetric measurements. Calorimetric measurements are essential to the latent heat characterization of PCMs. DSC [see Figs. 2(a) and 2(b)] is the most common calorimetric measurement method for determining the latent heat of carbon-based PCCs,^{67,68} and the t-history method is more commonly used for latent heat evaluation of larger or non-homogenous PCC samples [see Fig. 2(c)].⁶⁹ Other calorimetric methods, three-layer calorimetry (3LC),⁷⁰ and Peltier-element-based adiabatic scanning calorimetry (ASC) [see Fig. 2(d)],⁷¹ differ from DSC and the t-history method by their measurement principle, sample size, operating temperature, and calibration requirements [see Fig. 2(e)]. These methods have not yet been reported for characterizing carbon-based organic PCCs and, therefore, are omitted from discussion in this paper.

1. Differential scanning calorimetry

Differential scanning calorimeters, also commonly referred to as DSCs, are used to conduct DSC measurement, during which a sample crucible and an empty reference crucible are placed in the same controlled atmosphere and heated, cooled, or kept isothermal at the same temperature using resistive heating and compression or passive cooling.^{72,73} The difference in heat flow between the sample and reference is measured by sensors beneath both crucibles and plotted against the recorded temperature.⁷⁴

As outlined by ASTM Standard E793-06,⁷⁵ a typical dynamic DSC heating-cooling program, as shown in Fig. 3(a),⁶⁸ starts with an isothermal step, followed by a heating ramp, next by another isothermal step, then by a compressive cooling ramp or passive cooling, ending with a final isothermal step at the initial temperature.⁷⁶ A heat flow curve can be generated from this heating-cooling cycle. By integrating the area underneath a DSC peak, the latent heat of PCMs can be calculated, as shown in Fig. 3(b).⁷⁷ Factors contributing to the accuracy of the measured latent heat include the heating and cooling rates, sample size, and crucible selection. Typically, as recommended by ASTM Standard E793-06, the heating and cooling rates can be set to 10 °C/min. At this heating rate, there is sufficient time for DSC samples, typically with very small mass, to reach equilibrium while maintaining a high signal-to-noise ratio. At heating and cooling rates of over 10 °C/min, even small DSC samples of highly thermally conductive carbon-based organic PCCs may have difficulty reaching the quasi-equilibrium state for accurate latent heat measurements. For carbon-based PCCs containing organic PCMs with supercooling tendencies, such as caprylic acid and sugar alcohols, a much lower heating

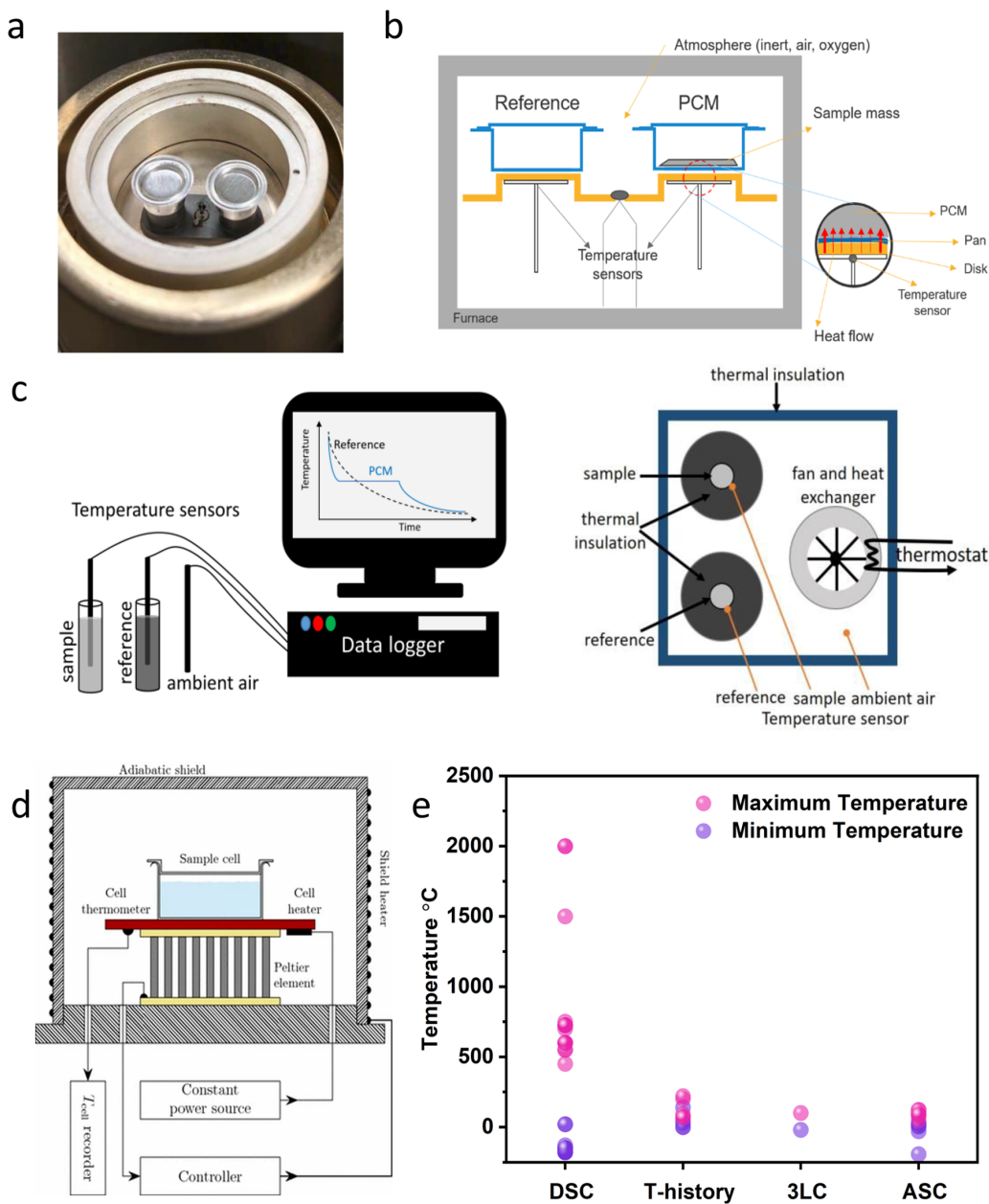
and cooling rate should be used to prevent falsely low latent heat of solidification measurements.⁷⁸ The sample size of carbon-based PCCs should also be carefully considered before measurements. The sample size should be as small as possible for homogenous samples to ensure a uniform sample temperature throughout the measurement, and the quasi-equilibrium state can be achieved during phase transitions.⁷⁸ However, it is common for carbon-based PCCs to have local heterogeneity.^{79,80} Therefore, actual samples should not be too small, which may not well represent the bulk PCC. Depending on the density of the carbon-based PCC samples, hermetically sealed metal crucibles with a sample holding capacity of 10–100 µl are recommended to be used.^{67,68} Open crucibles should not be used for samples that evaporate or decompose due to a potential of mass loss; hermetically sealed crucibles are preferred in the circumstances shown in Fig. 3(c). However, if the pressure inside of the crucible becomes too high due to PCM evaporation, the hermetic seal may rupture, causing a large endotherm in the DSC curve, altering the latent heat calculation results, as shown in Fig. 3(d). Therefore, the use of high-pressure hermetic crucibles may be considered for preventing crucible rupture [see Fig. 3(e)].^{77,81}

2. T-history method

Using similar resistive heating and temperature sensing techniques, the t-history method mainly differs from DSC due to its large sample size of 15–150 ml; larger sample sizes can be used since both the reference and sample materials are contained in test tubes.⁸² Compared to DSC, which is limited to smaller sample sizes of less than 100 mg, t-history is the preferred method for measuring the latent heat of heterogeneous carbon-based PCCs, especially when the carbon-based materials can lead to differing degrees of crystallization of the PCM in different regions of the bulk materials.

Insulated test tubes are preferred to ensure the reference, and the sample inside the tubes have the same thermal resistance to their environment. The test tubes are placed in a temperature-controlled container to heat up until both the reference, and the sample reaches a set temperature of T_0 . Quickly expose both test tubes to a temperature-controlled environment lower than T_0 and record the $T(t)$ curve of both the reference and the sample.⁸³ Therefore, a t-history plot can be obtained. From the t-history plot, the degree of supercooling, heat capacity, phase change temperature, and latent heat can be derived. For t-history setups, water is commonly used as the reference material, indium is the temperature calibration material, and the temperature measurement range is typically from –40 to 200 °C.^{67,84,85} However, t-history setups have not yet been commercialized.⁶⁸ Therefore, the reference and calibration materials may differ for each self-built setup, resulting in different operating temperature ranges.

In addition to its apparent sample size difference, unlike DSCs, the obtained heat flow to the t-history temperature curve is not dependent on the heating rate. The signal-to-noise ratio of t-history plots is higher than that of DSC plots, allowing for less uncertainty in phase change temperature and latent heat measurement.^{86,87} Therefore, it is the preferred method for performing comparative studies of latent heat between carbon-based PCCs with relatively small composition variations. Moreover, the overall setup and operation price of a t-history setup is much lower than operating commercial DSCs.⁸⁸ However, despite these advantages, there are several limitations to using the t-history method. These include the long time needed to run the heating and cooling cycle and the narrow operational temperature



24 October 2024 0:08:43:27

FIG. 2. (a)–(c) DSC and t-history characterization of carbon-based organic PCCs.⁶⁸ (a) Image of crucibles in a DSC chamber, (b) schematic of crucibles and sensors inside a DSC chamber and (c) schematic of t-history method set up. Reproduced with permission from Fatahi *et al.*, Appl. Sci. 12(23), 12019 (2022). Copyright 2022 Authors, licensed under a Creative Commons Attribution (CC-BY 4.0) license. (d) Schematic of Peltier-element-based adiabatic scanning calorimeter chamber.⁷¹ Reproduced with permission from Leys *et al.*, Mater. Renew. Sustain. Energy 5(4) (2016). Copyright 2016 Springer. (e) Operating temperature comparison of common calorimetry methods.

range of a t-history setup compared to a DSC.^{68,89} Finally, the lack of available commercialized t-history systems also constrains their application as a leading method for accurate measurement of latent heat of carbon-based PCCs, which are dominated by dynamic DSC measurements.

III. ORGANIC PHASE CHANGE MATERIALS AND THEIR CARBON-BASED COMPOSITES

PCMs for typical TES applications can be classified into two main categories: inorganic and organic PCMs. Inorganic PCMs, including molten salt and salt hydrates, were developed in the early

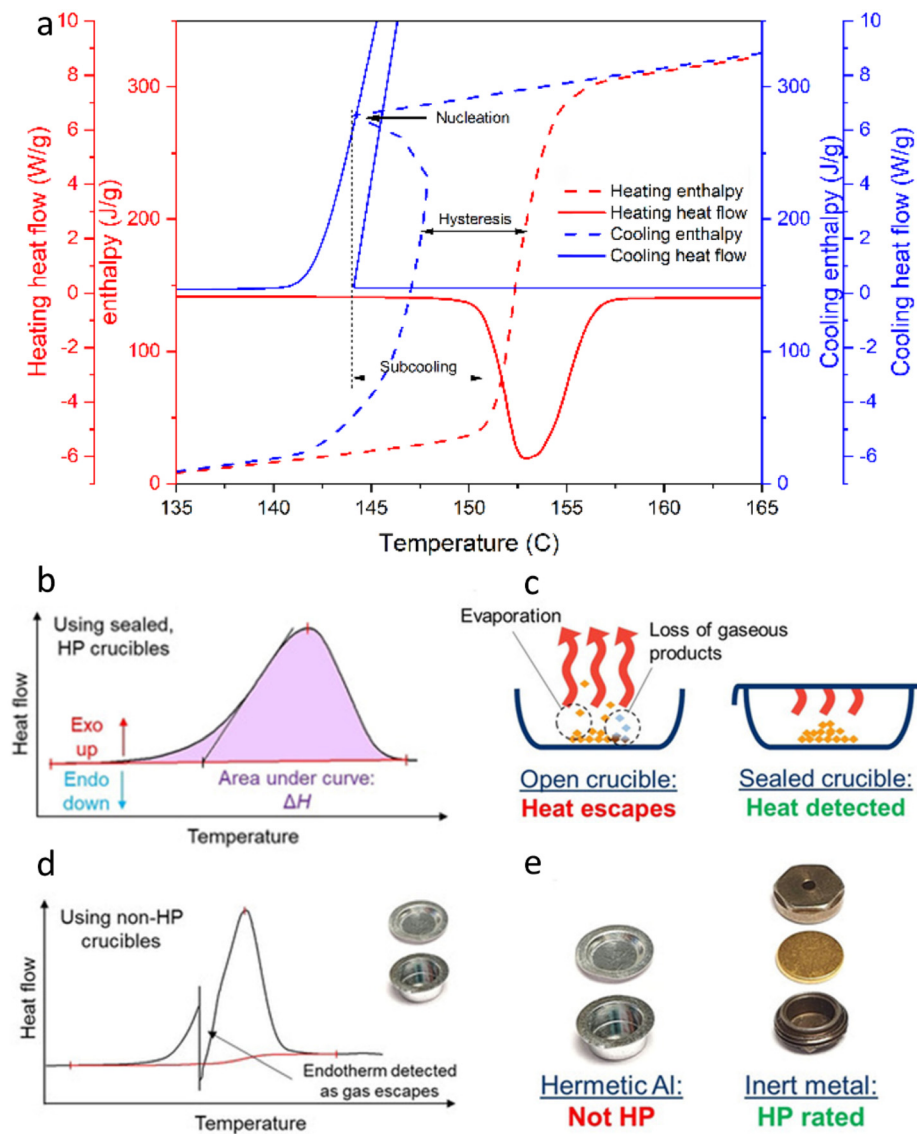


FIG. 3. (a) Stored heat and heat flow as a function of temperature during the melting phase and solidification.⁶⁸ Reproduced with permission from Fatahi *et al.*, Appl. Sci. **12** (23), 12019 (2022). Copyright 2022 Authors, licensed under a Creative Commons Attribution (CC-BY 4.0) license. (b)–(e) Analysis of the DSC characterization using hermetically sealed and non-hermetically sealed crucibles.⁷⁷ (b) Determination of the latent heat of an exothermic decomposition by integrating under its DSC curve; (c) comparison of open and closed crucibles; (d) a large endotherm registered in DSC plot due to rupture of the crucible's hermetic seal; and (e) comparison of non-high-pressure and high-pressure crucibles. Reproduced with permission from Green *et al.*, Angew. Chem. Int. Ed. **59** (37), 15798 (2020). Copyright 2020 John Wiley & Sons.

20th century. They generally have sizeable latent heat, reasonable thermal conductivity, and are non-flammable. However, their high density, large degree of supercooling, high corrosiveness, tendency for phase separation, and chemical and thermal instability have made them unsuitable for many TES applications. Since the mid-20th century, organic PCMs, including paraffin, fatty acids, fatty alcohols, and PEG, have been widely used in most TES applications thanks to a number of favorable attributes.⁵ Like inorganic PCMs, organic PCMs also have relatively high latent heat. However, they generally have the advantages of high abundance, low cost, low density, no phase separation, minimal supercooling, high biocompatibility, high chemical stability, and moderate phase change temperatures ranging between 25 and 85°C, depending on the length of their carbon chains.⁹⁰ Only sugar alcohols differ from other organic PCMs by having higher phase change temperatures and larger degrees of supercooling.⁹¹

Despite having many favorable characteristics, low thermal conductivity and leakage are two main drawbacks for organic PCMs. Other non-phase-changing materials are often composited with organic PCMs to overcome the drawbacks. Carbon materials are commonly selected due to their high thermal conductivity, low density, good wettability, tunable function surface, and high visible solar radiation absorption rate.⁶⁴ Carbon materials can be categorized according to their dimensions, as shown in Fig. 4(a). The selection of a particular carbon material for compositing with PCMs depends on the desired functionality the carbon material can add to the PCC. For example, CNTs and graphene have ultrahigh thermal conductivities and very high absorption of visible light, making them suitable for PCC for solar-thermal harvesting applications, as shown in Fig. 4(b).^{92–94} GO can be easily prepared and has excellent interfacial interactions with organic PCMs.⁵ Expanded graphite (EG) can also be easily prepared

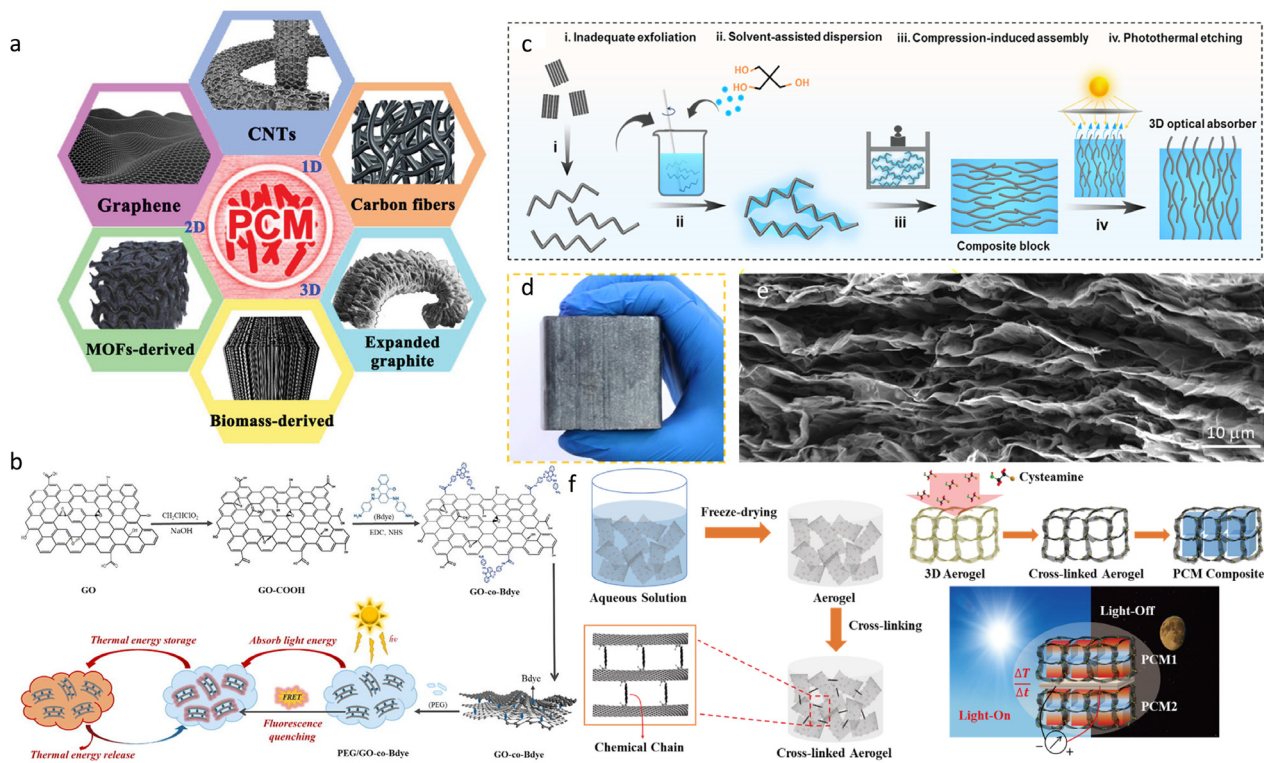


FIG. 4. (a) Carbon materials of various dimensions for compositing with PCMs.⁶⁴ Reproduced with permission from Chen *et al.*, *Adv. Sci.* **8**(9), 2001274 (2021). Copyright 2021 John Wiley & Sons. (b) The preparation process of PEG/GO-co-Bdye (blue anthraquinone dyes) PCC.⁹⁴ Reproduced with permission from Wang *et al.*, *Chem. Eng. J.* **428**, 130605 (2022). Copyright 2022 Elsevier. (c)–(e) Fabrication and morphology of WEG/TME;⁹⁵ (c) The preparation process of WEG/TME (worm-like expanded graphite/trimethylololethane) PCC; (d) Digital image of WEG/TME; and (e) SEM image of WEG/TME. Reproduced with permission from Wu *et al.*, *ACS Appl. Mater. Interfaces* **13**(16), 19200 (2021). Copyright 2021 American Chemical Society. (f) The preparation of cysteamine cross-linked graphene aerogel (GA)-based PCCs.⁹⁷ Reproduced with permission from Yu and Song, *Materials* **15**(13), 4541 (2022). Copyright 2022 Authors, licensed under a Creative Commons Attribution (CC-BY 4.0) license.

and has a porous and worm-like structure. EG has high thermal conductivity and a large surface area, allowing for good organic PCMs adsorption as shown in [Figs. 4(c)–4(e)].^{11,95} EG is also a carbon-based material reported to endow flame-retardant properties to organic PCMs.⁹⁶ Carbon foams, graphene foams, and GAs have interconnected, highly porous network structures as shown in Fig. 4(f).^{3,97} Capillary force and hydrogen bonds can hold liquid PCMs with minimal leakage, while the network structures enhance the thermal conductivity and the mechanical properties of their PCCs.²⁵

IV. LATENT HEAT ENHANCEMENT

Due to their high latent heat, organic PCMs are particularly attractive for thermal energy storage applications. Endothermic and exothermic peaks in dynamic DSC curves correspond to the fusion and solidification of the PCM. The transition onset, peak transition, and end of the transition can be found at the peaks' beginning, maximum, and end, respectively. The latent heat, or phase transition enthalpy, can be calculated by integrating the area under the heat flow curve.

Theoretically, organic PCMs can provide ample thermal energy storage capacity in quasi-isothermal conditions. However, their low thermal conductivity usually severely hinders their actual applications. Therefore, organic PCMs are commonly composited with carbon-

based materials to enhance their thermal conductivities. However, the addition of carbon in PCCs leads to a decrease in the weight percentage of their PCMs, often leading to a decrease in the latent heat of the PCCs to the pure PCMs.¹⁶ In many circumstances, with dispersed particulate PCCs, in particular, the addition of carbon will even disproportionately contribute to the decrease in latent heat of the PCC due to the carbon-based material hindering the crystallization of the PCM.⁹⁸

A number of early research have focused on controlling the decrease in the latent heat of the PCC so that it is proportional to the weight increase in the carbon-based material.^{99,100} However, with the recent diversification of carbon-based organic PCCs, it has been discovered that some carbon materials could increase the PCCs' latent heat compared to pure PCMs through various means. The latent heat enhancement mechanisms of carbon-based materials can be summarized into four main categories, including the promotion of PCM crystallization during solidification, compressive stress during PCM melting, the introduction of attractive intermolecular forces between the PCM and carbon-based materials, and the formation of hydrogen bonds within the PCM. Table I summarizes the latent heat enhancement methods reported in the literature and the degrees of enhancement. A few other mechanisms have been proposed to explain instances where the latent heat increase cannot be easily elucidated by the four main mechanisms, including changes in crystallization rate

TABLE I. Comparison of the latent heat enhancement ratio of various carbon-based organic PCCs.

PCM	PCC	Pure PCM latent heat, Δh_{pcm} (J g ⁻¹)	PCC latent heat Δh_{pcc} (J g ⁻¹)	Latent heat enhancement (%)	Reference
Paraffin	Paraffin/CNT sponge	136.0	138.2	1.62	20
Paraffin	Paraffin/carbon aerogel	172.2	185.6	7.78	21
1-octadecanol	1-Octadecanol/hollow rGO tube	237.0	262.5	10.8	22
PEG	PEG/CNT/chitosan/PVA	150.0	150.9	0.60	23
Docosane	Docosane/spongy graphene	256.1	262.8	2.62	101
PEG	PEG/HGA	171.0	173.8	1.64	102
PEG	PEG/BNNT/rGO	188.5	195.6	3.77	107
Paraffin	Paraffin/EG	131.8	135.7	2.95	108
Shell wax	Shell wax/SWCNT	156.3	176.6	13.0	109
Shell wax	Shell wax/MWCNT	156.3	172.1	10.1	109
Shell wax	Shell wax/CNF	156.3	166.9	6.78	109
PW	PW/MWCNT	165.3	165.4	0.06	111
Paraffin	Paraffin/aligned-CNT (a-CNT)	196.5	218.6	11.2	112
AZO	AZO/rGO	147.6	496.8	237	114

and increased phonon absorption by the PCM.^{20,23,24} However, these other mechanisms either do not have enough support from experimental results or lack detailed theoretical reasoning. The evaluation of the latent heat enhancement mechanism is especially complicated because, as discussed in the previous section, certain discrepancies in the inputs, such as heating rate and sample size, during characterization may lead to the latent heat being biased. False cases of latent heat enhancement may be reported, while genuine cases of latent heat enhancements with novel mechanisms may be overlooked if these biases are not correctly addressed. A consensus on which mechanisms can potentially lead to a PCC having higher latent heat than its PCM component has not yet been reached. Members of the scientific community dispute a number of the proposed mechanisms.

A. Enhanced crystallization

Researchers have made the connection between latent heat decrease with lower degrees of crystallization since the early studies on the shape stabilization and thermal conductivity of organic PCMs using nano-dispersed carbon particles hindered PCM crystallization and resulted in significant declines in the latent heat of the PCM. However, until recently, it has been a challenge to promote the crystallization of organic PCMs beyond that in their pure state through compositing carbon-based materials.

In 2014, Li *et al.*¹⁰¹ demonstrated that small amounts of spongy graphene sheets could act as nucleating agents, promote docosane crystallization, and increase its latent heat from 256.1 J g⁻¹ to 262.8 J g⁻¹. Sharper XRD peaks of docosane were observed when spongy graphene sheets were added, indicating the promotion of docosane crystallization. Subsequently, Yang *et al.*¹⁰² also demonstrated that by compositing PEG with a GO aerogel and hybrid GO/graphene nanoplatelet (GNP) aerogels (HGAs) [see Figs. 5(a)-5(g)], the latent heat of PEG could increase from 171.0 J g⁻¹ to 173.1 J g⁻¹ and 173.8 J g⁻¹, respectively, due to the promotion of PEG crystallization by the aerogels. The crystal structure of the original PCM is not altered by carbon-based materials in the studies conducted by both Li *et al.* and Yang *et al.*^{101,102}

Compared to promoting crystallization through nucleation, the self-alignment of alkane and its derivatives along the surface of large graphene flakes results in even better crystallization results and more significant increases in latent heat. As reported by Warzoha and Fleischer,¹⁰³ adding 15 μm diameter graphene flakes to paraffin increased the latent heat by 11%. Moreover, by applying molecular mechanics modeling, Barnard and Matzger,¹⁰⁴ discovered that the absorption of 1-octadecanol and 1-octadecanethiol on a graphite surface results in the 1-octadecanol and 1-octadecanethiol molecules orienting in a zigzag pattern instead of the linear pattern seen in their freestanding crystals as shown in Fig. 5(h). These zigzag oriented molecules form contracted lattices with higher lattice energies than their freestanding counterparts, as shown in Fig. 5(i). This molecular mechanic modeling derived lattice energy corresponds closely proportional to the enthalpy of absorption characterized through flow microcalorimetry experiment. Following the work of Barnard and Matzger, our group demonstrated with XRD that when 1-octadecanol is filled into the hollow rGO tubes (HrGOTs) through vacuum impregnation, as shown in Fig. 5(j), the 1-octadecanol adsorbed on the smooth inner surface of HrGOTs will have right-shifted peaks corresponding to contracted lattices with higher lattice energies shown in Fig. 5(k).²² The higher lattice energy of the adsorbed 1-octadecanol results in the HrGOT/1-octadecanol composite having a latent heat of 262.5 J g⁻¹ compared to 237.0 J g⁻¹ of as purchase 1-octadecanol; therefore, reporting an impressive 10.8% increase.

Crystallization of organic PCMs in carbon-based organic PCCs can also be promoted by adding metal-organic frameworks. These frameworks often show a strong affinity for organic PCMs and increase their loading ratios when composited with the same 3D carbon-based assembly. Dong *et al.*¹⁰⁵ demonstrated that by adding a hierarchical zeolitic imidazolate framework, the absorption of PEG into a carboxyl-modified carbon cloth scaffold was boosted from 54 wt. % to 63 wt. %. In turn, the carboxyl-modified carbon cloth scaffold acted to prevent the inhibition of the crystalline-amorphous phase transition of the PEG by the hierarchical zeolitic imidazolate

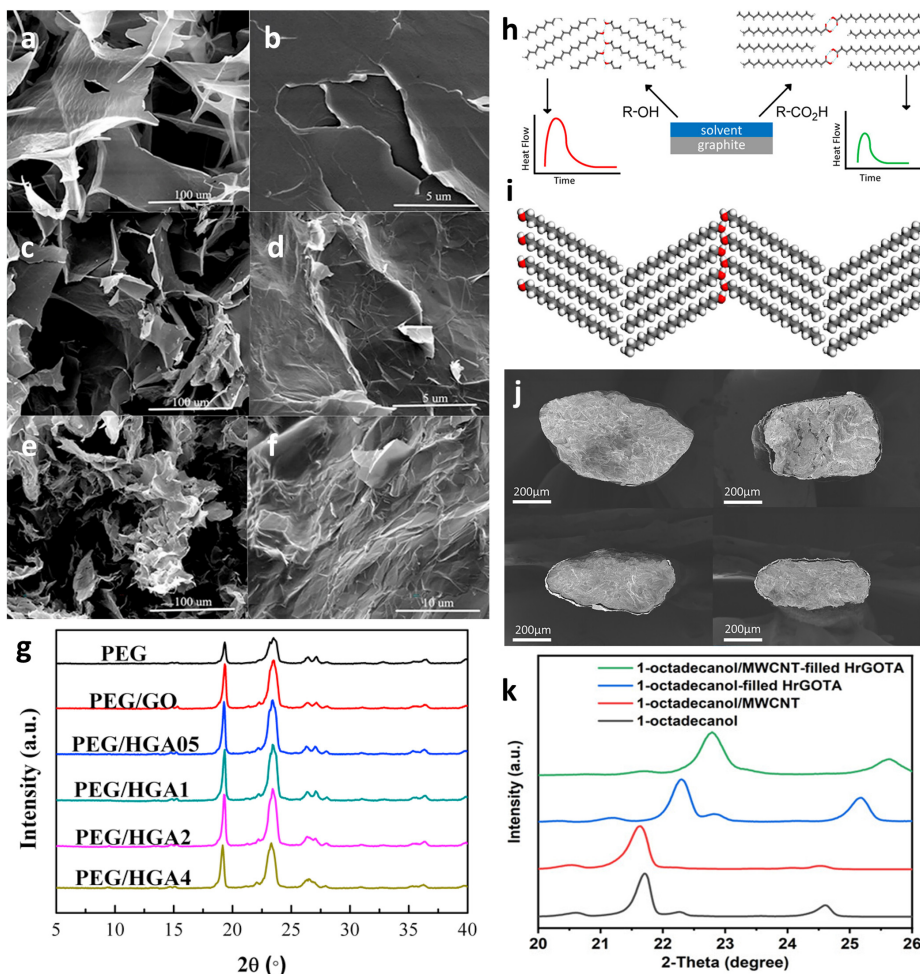


FIG. 5. (a)–(g) GO and HGA-based PCCs:¹⁰² (a) and (b) SEM images of GO and PEG/GO; (c) and (d) SEM images of HGA05 and PEG/HGA05; (e) and (f) SEM images of HGA2 and PEG/HGA2; and (g) XRD patterns of pure PEG, PEG/GO, and PEG/HGAs. (Carbon weight ratio: PEG/HGA05<PEG/HGA1<PEG/HGA2<PEG/HGA4). Reproduced with permission from Yang *et al.*, Carbon **100**, 693 (2016). Copyright 2016 Elsevier. (h) and (i) Molecular packing of organic PCMs on graphite.¹⁰⁴ (h) Impact of molecular packing of R-OH and R-COOH on graphite surfaces on their solidification enthalpies; and (i) a molecular model of the packing pattern of 1-octadecanol on graphite. Reproduced with permission from Barnard and Matzger, Langmuir **30**(25), 7388 (2014). Copyright 2014 American Chemical Society. (j) and (k) HrGOT-based 1-octadecanol PCCs:²² (j) SEM images of HrGOT/1-octadecanol; and (k) right shift of the XRD patterns of the hollow rGO tube assembly (HrGOTA) composites filled with 1-octadecanol and 1-octadecanol/MWCNTs compared to 1-octadecanol and 1-octadecanol/MWCNTs. Reproduced with permission from Li *et al.*, ACS Appl. Mater. Interfaces **15**(15), 18940 (2023). Copyright 2023 American Chemical Society.

framework. As a result of the synergetic effect of the hierarchical zeolithic imidazolate framework and the carboxyl-modified carbon cloth scaffold, the latent heat of the PCC can reach up to 119.6 J g^{-1} compared with 104.1 J g^{-1} of the PCC consisting of only PEG and the carboxyl-modified carbon cloth.

B. Compressive stress

Organic PCMs are often impregnated into porous materials for shape stabilization during phase transition. Several studies have revealed that the impregnation of organic PCMs in microporous materials yields higher latent heat than impregnation in nanoporous materials.¹⁰⁶ Generally, microscaled pores do not hinder the crystallization of the impregnated PCM.

Furthermore, when the micropores are tailored with the suitable material and geometry, the PCC's latent heat can exceed that of the pure PCM. Cheng *et al.*²³ fabricated a CNT/chitosan (CS)/poly(vinyl alcohol)(PVA) folded layer-bridge network structure using directional freezing. After impregnating the microporous network with PEG, the latent solidification heat of the resulting PCC reaches 150.9 J g^{-1} , compared to 150.0 J g^{-1} of pure PEG. The increase in solidification latent

heat is attributed to the compressive stress of the network structure on the PEG, which slows down the solidification process by lowering the cooling rate. The lower cooling rate can promote more PEG molecules to crystallize. The compressive stress of the network on the PEG also prevents the PCC's latent heat from being affected by external mechanical bending, opening the door to potential applications of mechanically stable PCCs with high latent heat.

Similarly, Wang *et al.*¹⁰⁷ fabricated a boron nitride nanotube (BNNT) aerogel reinforced by rGO. Having a similar network structure as the CNT/CS/PVA by Cheng *et al.*, when impregnated with PEG, the PCC's latent heat increases to 195.6 J g^{-1} , compared to 188.5 J g^{-1} of pure PEG. The latent heat increase is also concluded as the compressive stress of the aerogel hindering the rate of fusion and solidification by Wang *et al.*, who cited Cheng *et al.*, though Wang *et al.* speculated C-H \cdots π intermolecular interaction as the primary contributor to the latent heat increase.

In another study, Chen *et al.*²⁰ adopted a CNT sponge as a porous scaffold to encapsulate paraffin wax (PW). The resulting PCC with 91 wt. % PW loading has a latent heat of 138.2 J g^{-1} , compared to pure PW with a latent heat of 136.0 J g^{-1} . Chen *et al.* reasoned that the compressive stress of the CNTs on the melting PW during its volume

expansion could work in conjunction with extensive C-H $\cdots\pi$ interactions between the CNTs and PW to cause the increase in latent heat.

The contribution of compressive stress of carbon-based materials on the latent heat increase in PCCs, however, is not accepted by Xia *et al.*,¹⁰⁸ who found that expanded graphite (EG)/paraffin PCCs exhibited lower latent heat than pure paraffin. Xia *et al.* argued that the lower latent heat of the PCC was caused by the compressive pressure of the EG on the melting paraffin, which restricted the molecular thermal motion of the paraffin.

C. Intermolecular attraction

At the molecular level, the interaction potential energy held between different molecules in a material ultimately determines the latent heat of the material.¹⁰⁹ Enhancing crystallization and applying compressive stress can increase the potential energy between PCM molecules in a PCC. However, this potential energy does not have to be only between PCM molecules; it could also be between PCM molecules and the molecules of carbon-based materials in the PCC. By adding carbon-based materials whose molecules have higher potential energies with PCM molecules than the potential energy between pure PCM molecules, the latent heat of the PCC can be engineered to be higher than in pure PCMs.

High potential energies between carbon-based molecules and PCM molecules are most commonly achieved by introducing intermolecular interactions, such as C-H $\cdots\pi$ interactions.¹⁷ Shaikh *et al.*¹⁰⁹ first discovered that by dispersing small volume fractions (0.1% to 1%) of single-wall CNTs (SWCNTs), multiwall CNTs (MWCNTs), and carbon nanofibers (CNFs) into PW, the latent heat of the resulting PCC becomes higher than pure PW. A theoretical model was established

correlating the attractive potential between the carbon-based molecules and the PW molecules and the latent heat of the PCC. The change in latent heat ΔH can be expressed by the following:¹⁰⁹

$$\Delta H = \rho_{PCM} \int \int_{PCM} w(x, y) dx dy, \quad (5)$$

where $w(x, y)$ is the Lennard-Jones potential. As mentioned by Israelchvilli,¹¹⁰ the attractive contribution is greater than the repulsive contribution in $w(x, y)$ when C-H $\cdots\pi$ interactions are involved. By performing numerical simulations using Eq. (5), it was confirmed that the latent heat increases of the PCCs compared to pure PW found from DSC experiments correspond closely to the values estimated by the theoretical model, with the PCC dispersed with 1% 1 nm diameter SWCNT achieving a latent enhancement of up to 13.0%. The latent heat enhancement of the PCC with 1% 10 nm diameter MWCNT and 1% 100 nm diameter CNFs were at 10.1% and 6.8%, respectively. The difference in enhancement rate is attributed to the larger molecular density, larger surface area, and better dispersion of the SWCNTs, which results in greater intermolecular attraction. These criteria for greater intermolecular attraction are confirmed by Wang *et al.*¹¹¹ in their study on MWCNT/paraffin PCCs, in which a much smaller latent heat enhancement of 0.1 J g $^{-1}$ was observed for PCCs with 0.2 wt. % MWCNTs compared to pure paraffin.

Direct experimental evidence of C-H $\cdots\pi$ interaction in promoting higher latent heat in PCCs than in pure PCMs was found by Chen *et al.*²⁰ In their study of CNT sponge/PW composites [see Figs. 6(a) and 6(b)], high-energy XRD was employed to obtain the pair distribution function data, which was used to analyze the interaction type and intermolecular distance between CNT molecules and paraffin

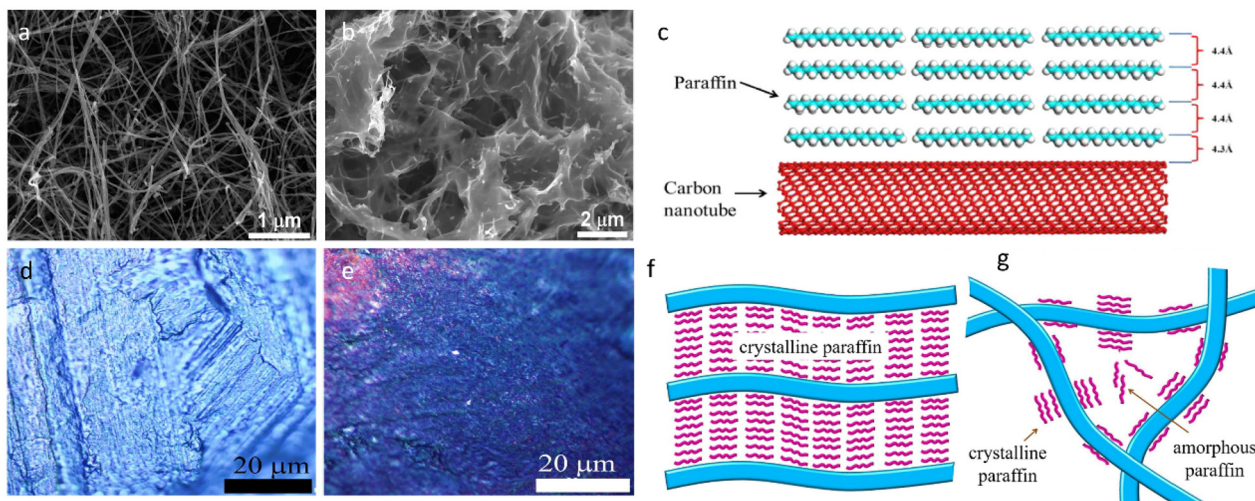


FIG. 6. (a)–(c) C-H $\cdots\pi$ intermolecular interaction induced latent heat enhancement in CNT-based PCCs:²⁰ (a) SEM image of the inner part of the CNT sponge showing a highly porous structure; (b) SEM image of the PCC showing the presence of PW in the CNT sponge pores; and (c) illustration of the PW molecules with an intermolecular distance of 4.4 Å and a smaller interfacial distance of 4.3 Å to an adjacent CNT due to the presence of C-H $\cdots\pi$ intermolecular interaction. Reproduced with permission from Chen *et al.*, ACS Nano 6(12), 10884 (2012). Copyright 2012 American Chemical Society. (d)–(g) CNT alignment induced latent heat enhancement in CNT-based PCCs:¹¹² (d) Polarizing microscopy of 85 wt. % paraffin @ a-CNT PCC, displaying an apparent alignment of paraffin triggered by the C-H $\cdots\pi$ intermolecular interaction between PW and CNTs; (e) polarizing microscopy of 85 wt. % paraffin @ random-CNT (r-CNT) PCC, displaying a much more uniform morphology; (f) illustration of paraffin molecules around the a-CNT surfaces and the further evolution for the crystallization of paraffin molecule induced by C-H $\cdots\pi$ intermolecular interaction; and (g) illustration of paraffin molecules around r-CNT, forming limited crystallization. Reproduced with permission from Zhu *et al.*, Appl. Energy 254, 113688 (2019). Copyright 2019 Elsevier.

molecules. The C–C bonds of CNTs and paraffin remain unchanged in the low r range of 1 to 4 Å. A van der Waals peak at 4.4 Å represents the distance between adjacent paraffin molecules, however, at the interface between paraffin and CNTs, the van der Waals peak shifts to 4.3 Å as shown in Fig. 6(c). It is this peak shift that suggests remarkable intermolecular C–H··· π interactions between the paraffin and CNT molecules at their interfaces.

Zhu *et al.*¹¹² fabricated an aligned CNT/paraffin composite and also found that the latent heat of PCC with 93 wt. % paraffin loading had a latent heat of 218.6 J g⁻¹, compared to the latent heat of 196.5 J g⁻¹ of pure paraffin. The 11.2% latent heat increase was also attributed to the presence of C–H··· π interactions between the CNTs and the paraffin molecules. Zhu *et al.* further elaborated that the C–H··· π interactions may make the paraffin molecules align more easily and consequently affect their adjacent paraffin molecules, therefore enhancing the long-range crystallization of paraffin in the PCC [see Figs. 6(d)–6(g)].

Due to the large surface area and good dispersion capability of CNTs, CNT-based PCCs makeup the majority of PCCs whose latent heat enhancement can be attributed to an enhanced intermolecular attraction. Wang *et al.*¹¹³ however, were able to successfully enhance the latent heat of “graphene-like” carbon/paraffin PCC with 91.7 wt. % paraffin loading to 104.5% of that of pure paraffin. This enhancement was achieved by ensuring the “graphene-like” carbon was specifically fabricated to have a very large surface area and sufficiently dispersed. Nitrogen Brunauer–Emmett–Teller (BET) adsorption and desorption isotherms of the mesoporous carbon revealed the presence of a hierarchy of pore sizes ranging from micro to macro. The pore-in-pore structure of the “graphene-like” carbon guarantees its large surface area of up to 1101 m² g⁻¹, which supports the establishment of C–H··· π type intermolecular interactions between itself and paraffin molecules similar to that between CNT and paraffin molecules.

D. Hydrogen bonding

In addition to C–H··· π interactions, another typical intermolecular interaction that is commonly established for PCM molecules is hydrogen bonding. Depending on the specific hydrogen bonding formed on the PCM, the latent heat of the resulting PCC can be enhanced.¹¹⁸

Luo *et al.*¹¹⁴ fabricated an azobenzene chromophore (AZO)/rGO PCC with the capability of absorbing light in the ultraviolet-visible range and releasing heat based on reversible *E*-to-*Z* isomer transition as shown in Figs. 7(a) and 7(b), which is a special type of phase change. With the help of aryl radicals, AZOs are grafted rGO molecules via hydrogen bonding. Each AZO *Z* isomer forms a single hydrogen bond with rGO, while each AZO *E* isomer forms two hydrogen bonds with rGO. At temperatures between 42 and 94 °C, an *E*-to-*Z* isomer transition occurs, and the formation of an extra hydrogen bond per AZO molecule results in a large exothermic heat flow. The latent heat of the AZO/rGO PCC is over 3.3 times larger than that of pure AZO [see Figs. 7(c) and 7(d)].

The latent heat of solid-liquid phase change can also be indirectly enhanced by introducing hydrogen bonds. Tan *et al.* reported that after modifying calcium chloride hexahydrate (CCH) with lotus root starch (LRS), its PCC with EG exhibits a latent heat 13.3% higher than that of CCH/EG.¹¹⁵ The LRS interacts with the CCH through hydrogen bonds. LRS contains many hydrophilic groups, which allows it to

form a hydrophilic coating on the inner EG surface. The water retention in CCH is improved when made into a composite with EG and the latent heat of LRS-modified CCH/EG PCC is higher than that of CCH/EG.

Compared to achieving latent heat enhancement of PCCs through directly introducing C–H··· π interactions, many studies have shown that directly introducing hydrogen bonds between PCMs and carbon-based materials will deteriorate the latent heat of the PCC during solid-liquid phase change processes.¹¹⁸ Unique phase change processes or a third non-PCM, non-carbon-based material needs to be introduced to employ hydrogen bonding in PCC latent heat enhancement.

V. SHAPE STABILITY ENHANCEMENT

Organic PCMs are some of the most extensively utilized latent heat storage materials. However, leakage during the solid-liquid phase transition can cause severe material loss and contamination.²⁵ The efficient and sustainable use of PCM for thermal storage applications requires PCMs to be stabilized during solid-liquid phase transition. The mechanisms governing the effectiveness of PCM shape stabilization can be categorized as either geometric constraints or binding forces. When geometrically confined within a thermally stable enclosure, bound to a thermally stable solid structure by either force interactions (covalent bonding, hydrogen bonding, van der Waals force, or capillary force) or a combination of the two types of interactions, PCMs are stabilized and confined within a defined geometry. Carbon materials are abundant in different forms/allotropes range of varieties. Many of these varieties have geometries or exhibit physical or chemical interactions that promote the stabilization of PCCs.

Hot plate leakage tests, compression tests, and thermo-mechanical tests are often conducted to examine the shape stability of these carbon-based organic PCCs.³ Hot plate leakage tests are the most commonly conducted of the three types of tests.²⁶ During the hot plate leakage tests, PCCs are heated on top of filter paper on a hot plate to a temperature above the solid-liquid phase change temperature. Therefore, leakage of the PCC can be examined visually or by measuring the remaining weight.³¹ Compressive testing is often coupled with hot plate leakage testing, where weights are added on top of the PCC to examine the mechanical stability of the PCC at or above phase change temperatures.¹¹⁶ Thermo-mechanical testing is performed on a thermo-mechanical analyzer (TMA) for more quantitative results. Using a TMA, the three-dimensional volume change of the PCC under different temperature and load force conditions can be studied.¹¹⁷

It has been proven through various leakage evaluation tests that different strategies can be applied to effectively improve the phase stability and overall functional performance of organic PCMs incorporated with carbon additives. These methods include (a) microencapsulation, based on geometric confinement; (b) nano-material incorporation, based on microscopic binding forces; and (c) impregnation into porous materials, based on a combination of geometric confinement and binding forces.

A. Microencapsulation

Microencapsulation stabilizes organic PCMs and prevents leakage through geometric confinement. Commonly, PCM particles ranging from submicrometer to millimeter scales are individually covered by a shape-stable shell material that can ensure the confinement of PCMs in

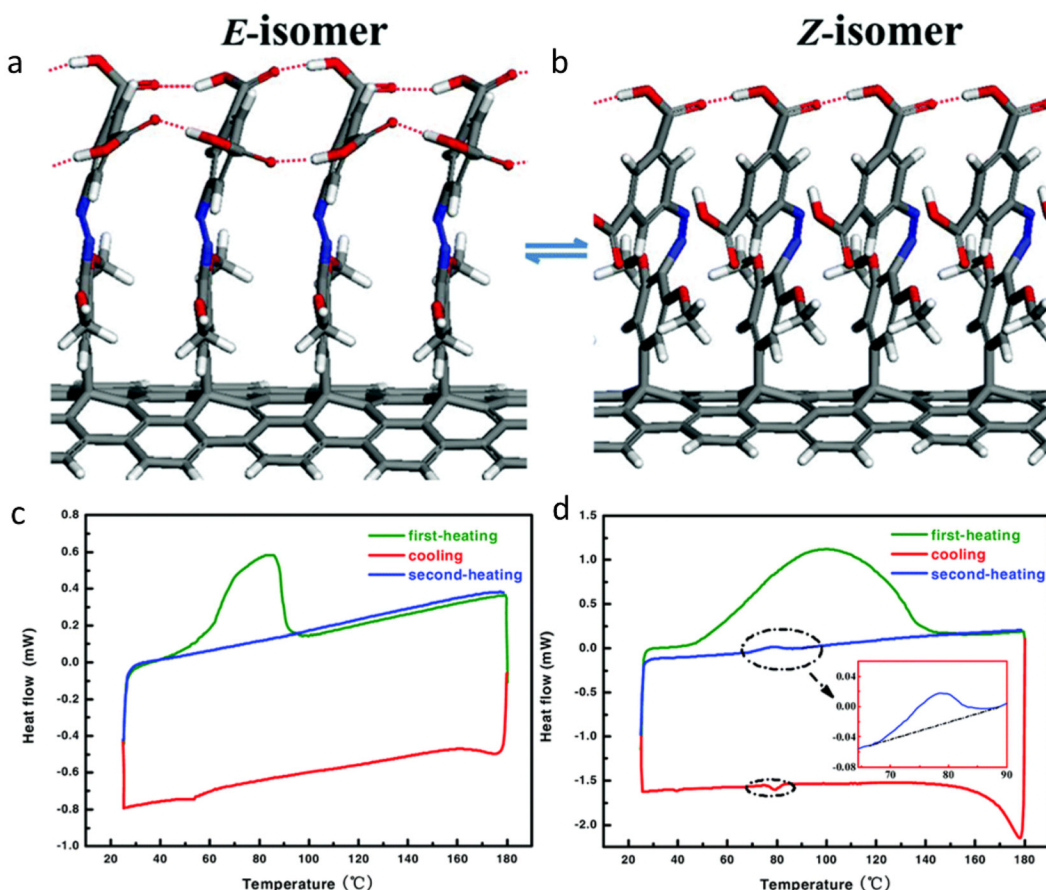


FIG. 7. (a)–(d) Latent heat enhancement via the introduction of hydrogen bonds between AZO molecules with the help of rGO.¹¹⁴ (a) stable model of E-isomer of AZO-rGO by density functional theory (DFT) calculations; (b) stable model of Z-isomer of AZO-rGO by DFT calculations; (c) DSC plot of AZO with first-heating(green), cooling (red) and second-heating (blue) periods; and (d) DSC plot of AZO-rGO with first-heating (green), cooling (red) and second-heating (blue) periods. Reproduced with permission from Luo *et al.*, *Nanoscale* 7(39), 16214 (2015). Copyright 2015 Royal Society of Chemistry.

24 October 2024 08:43:27

their liquid state. It is one of the earliest-developed and most widely applied shape-stabilizing methods. Various physical, chemical, and physicochemical methods have been developed for encapsulating organic PCMs. Depending on the desirable functionality and properties of the resulting PCCs, a wide range of organic and inorganic shell materials could be selected. Resins and other organic shell materials are selected for their low density, excellent corrosion resistance, and ease of fabrication. Meanwhile, robust mechanical properties and strong thermal stability motivate the selection of silica and other inorganic materials as shell material. With unique functional properties such as high thermal conductivity and high absorption of visible light, carbon allotropes such as CNTs are often added to complement both organic and inorganic shell-forming materials. The resulting PCCs will benefit from enhanced functional capabilities, including increased thermal energy conversion efficiency and a higher solar absorption rate.

However, shells made mostly or entirely of carbon materials are rarely reported to be used to encapsulate PCMs due to the difficulty in forming such structures. A chemical emulsion method was developed by Wu *et al.* to encapsulate paraffin in a melamine resin shell.¹¹⁸

The melamine resin-encapsulated paraffin was then dry mixed with carbon fillers such as flake graphite (FG), multilayer graphene (GNP), or EG. The mixture was then pressed under a pressure of 20 MPa. The pressure allows the carbon-based fillers to form a carbon network around the melamine resin-encapsulated paraffin, providing a second encapsulating layer, as shown in Figs. 8(a)–8(e). The shape stability of the resulting PCC was studied at 70 °C. After 20 min of heating, the paraffin in the control group had completely melted, yet only a slight trace of leakage was observed for the PCC, confirming that the dual microencapsulation structure effectively promoted shape stability.

Alternatively, direct encapsulation of PCMs by porous carbon microsphere was achieved by Ji *et al.*³⁰ Functionalized polystyrene (PS) nanoparticles were used as templates for polymerizing soluble starch through hydrothermal synthesis as shown in Figs. 8(f)–8(j). Porous carbon microspheres were obtained by calcinating the polymer products in a tube furnace at 550 °C for 12 h under nitrogen. n-Octadecane was vacuum-impregnated into the microspheres. No leakage was observed when the 80 wt. % n-octadecane samples were heated above the solid-liquid phase change temperature for n-octadecane for

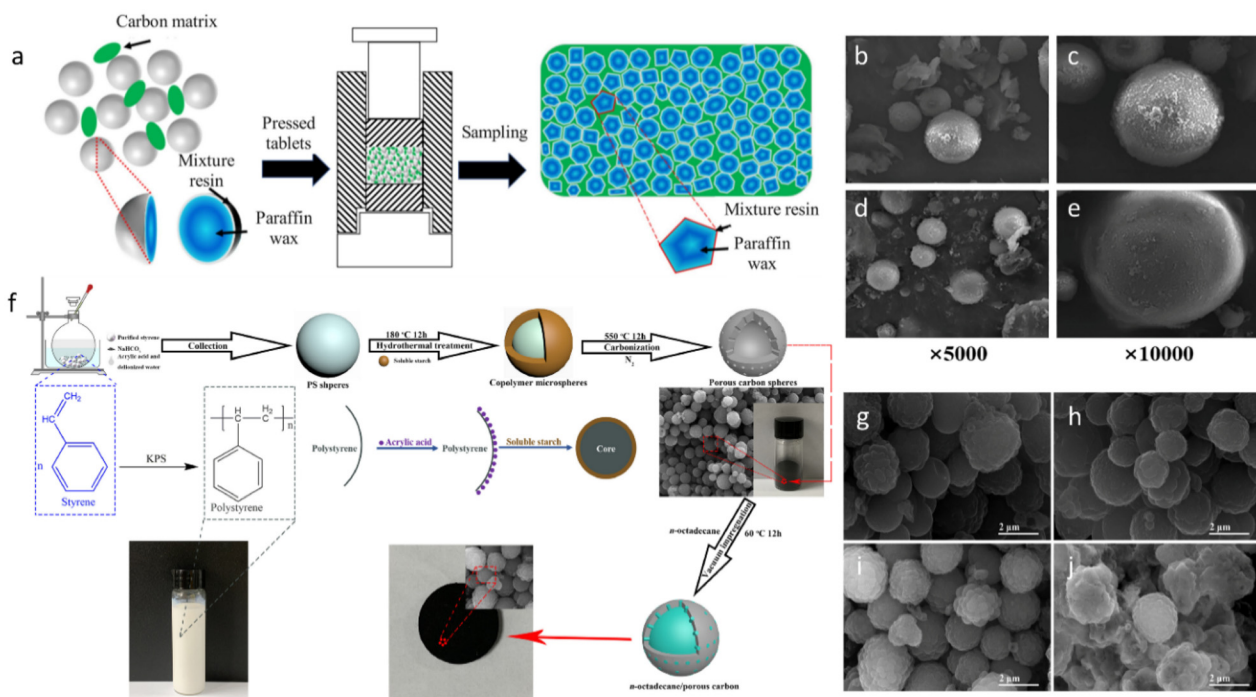


FIG. 8. (a)–(e) Shape stabilization of GNP/melamine/paraffin through microencapsulation.¹¹⁸ (a) Schematic of the preparation of carbon-filler microcapsule PCCs. (b) and (c) SEM image of GNP/melamine/paraffin microcapsule. (d) and (e) SEM image of EG/melamine/paraffin. Reproduced with permission from Wu et al., Appl. Therm. Eng. **212**, 118632 (2022). Copyright 2022 Elsevier. (f)–(j) Shape stabilization of n-octadecane/porous carbon through microencapsulation.³⁰ (f) Schematic of the preparation of the n-octadecane/porous carbon PCC; and (g)–(j) SEM images of the n-octadecane/porous carbon PCCs with different content of n-octadecane: (g) 50 wt. %, (h) 60 wt. %, (i) 70 wt. %, and (j) 80 wt. % Reproduced with permission from Ji et al., J. Energy Storage **27**, 101134 (2020). Copyright 2020 Elsevier.

24 October 2024 0:8:43:27

20 min. However, the PCC's 20.5% latent heat reduction compared to pure n-octadecane was measured.

Cao et al.²⁸ also developed a strategy for PCM microencapsulation through only carbon-based materials. O-phenylenediamine (oPD) was polymerized on the surface of SiO₂ nanoparticles. The SiO₂ was subsequently etched, and the oPD polymer was carbonized at 900 °C under a nitrogen atmosphere. The resulting porous carbon nanospheres coalesced into mesoscale structures with nano- and micropores. The mesoscale structures were directly immersed in tetradecyl amine (TDA), 1-hexadecanamine (HDA), and octadecyl amine (ODA) for impregnation. However, the shape stability of the PCCs was not investigated.

Full microencapsulation using organic or inorganic shells generally results in the lowest leakage rates of PCMs and the highest shape stability. A low leakage rate is also expected from PCMs encapsulated in carbon shells. However, more dedicated studies on the shape stability of carbon microencapsulated PCCs are needed to validate the effectiveness of carbon shells to improve shape stability. If the assumption stands, superior shape stabilities provided by carbon microencapsulation can help promote research on the fabrication of novel carbon shells, which could also be beneficial for other applications such as drug delivery.

B. Nano-material incorporation

Compared to forming shells for encapsulating PCM particles using carbon materials, it is much more convenient to form stable

PCCs by incorporating a wide variety of multidimensional carbon nano-materials and their derivatives. Dispersed carbon nano-materials have large surface areas to facilitate intermolecular and intramolecular interactions with organic PCMs. These interactions bind PCM molecules strongly to the dispersed carbon nano-materials. These carbon nano-materials are also bound to each other. As a result, a shape-stable PCC is formed. From a multidimensional perspective, 1D stabilization is achieved by filling PCMs into 1D hollow nanofibers [See Figs. 9(a)–9(e)];^{119–121} 2D stabilization traps PCMs between layers of nano-materials through interfacial interactions [see Fig. 9(f)],^{122,123} while 3D stabilization utilizes carbon nano-materials with nanoporous structure, into which molten PCMs can be vacuum impregnated.¹²⁴

Feng et al.²⁷ successfully filled lauric acid (LA) into MWCNTs with 5–10 nm diameters and lengths of 0.522 μm through a two-step diffusion and vacuum impregnation method. The PCC powder exhibited good shape stability after being heated to 80 °C for 20 min. The thermal conductivity of the PCC increased to about four times that of pure LA. However, the latent heat of the PCC was significantly compromised, with only 31.2% of pure LA. Due to the significant negative impact on the PCC's latent heat, it is rare to achieve PCC shape stabilization by incorporating PCM into hollow CNTs.

Graphene and its derivatives are commonly incorporated for the 2D stabilization of PCMs. Zhang et al.¹²⁵ stabilized n-hexadecane in double-walled polystyrene/GO nanosheets by forming a Pickering emulsion using a modified GO solution mixed. The emulsion was

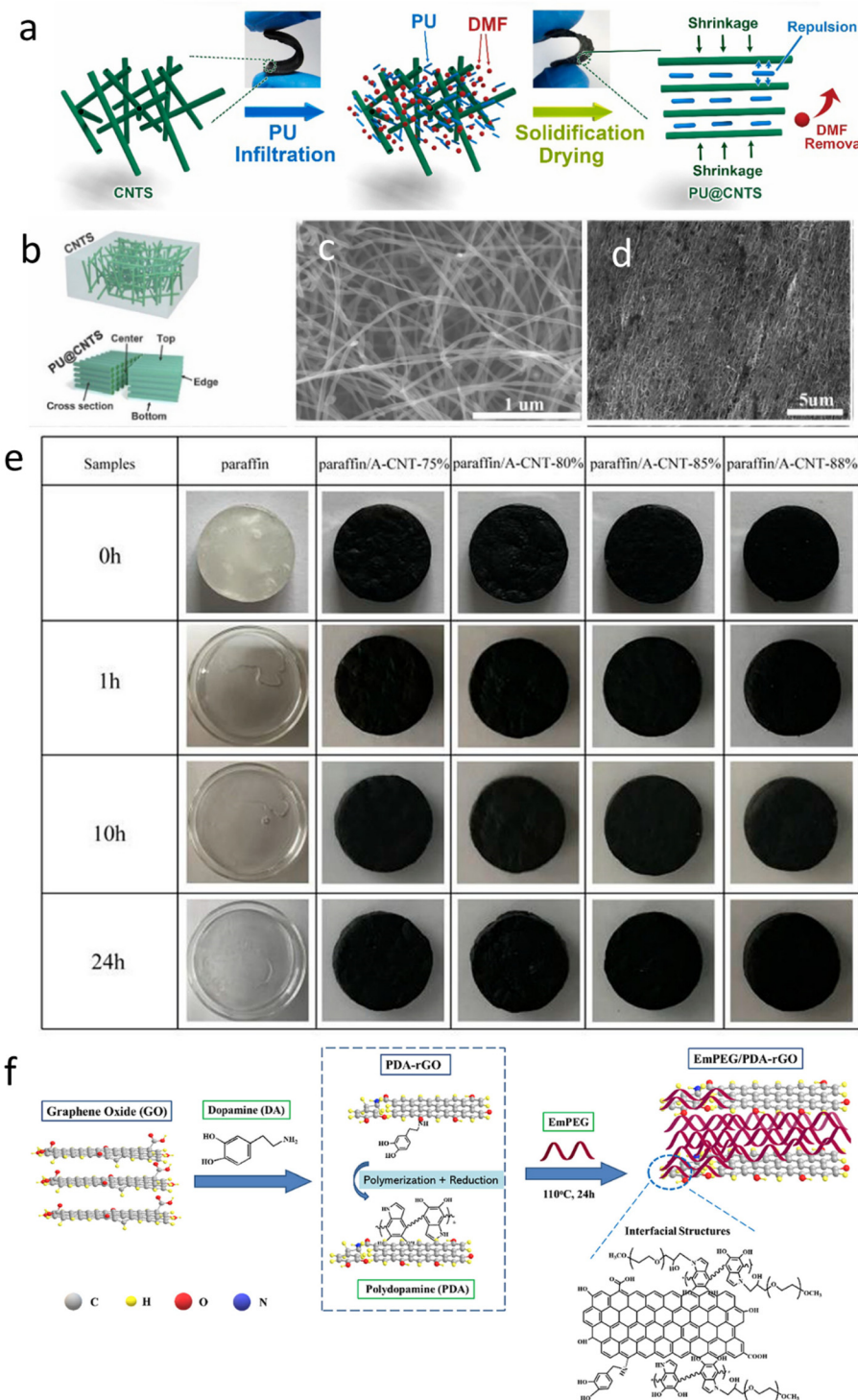


FIG. 9. (a)-(d) Shape stabilization of PU-based PCCs through CNTs (CNT sponge) incorporation:¹²⁰ (a) Schematic of the preparation of shape stable PU @ CNTS PCC; (b) schematic of interconnected CNTs in CNTs and different places in PU @ CNTS PCC; (c) SEM image of CNTs; and (d) SEM image of PU @ CNTS PCC. Reproduced with permission from Aftab *et al.*, Energy Storage Mater. **20**, 401 (2019). Copyright 2019 Elsevier. (e) Optical photographs of paraffin and paraffin/aggregated-CNT PCCs at 60 °C.¹²¹ Reproduced with permission from Han *et al.*, Ind. Eng. Chem. Res. **57** (39), 13026 (2018). Copyright 2018 American Chemical Society. (f) Schematic of the preparation process of EmPEG/PDA-rGO (epoxidized methoxy polyethylene glycol/polydopamine-reduced graphene oxide) PCC.¹²³ Reproduced with permission from Ge *et al.*, Sol. Energy Mater. Sol. Cells **208**, 110388 (2020). Copyright 2020 Elsevier.

polymerized at 68 °C for 16 h under a nitrogen atmosphere to form the PCC. Leakage and evaporation of the n-hexadecane were effectively prevented. Liu *et al.*¹²⁶ incorporated poly(styrene-co-maleic anhydride)-g-octadecanol (SMAC18) into a honeycomb-like structure

consisting of polymer and GO. With GO optimized to 2 wt. %, the PCC's size only experienced a minor 3.6% change even when heated up to 160 °C, while the shape-stability of pure SMAC18 significantly deteriorated at temperatures higher than 45 °C.

Instead of incorporating PCMs in structures consisting of 2D carbon-based materials, PCMs can also be stabilized by forming bonds with 2D carbon-based materials, such as GO, through grafting. For example, Liu *et al.*¹²⁷ grafted diethylene glycol hexadecyl ether (E_2C_{16}) onto GO through an esterification reaction with GO's carboxyl groups. The resulting PCC exhibited satisfactory shape stability where no significant size change and no leakage were observed when the samples with E_2C_{16} to GO mass ratios of 7:1. In addition to covalent bonding, the formation of hydrogen bonds or π - π stacking between PCMs and 2D carbon-based materials would also help with PCC stabilization. An excellent example of this is provided by Zhang *et al.*¹²⁵ who assembled PEG and GO into a brick-and-mortar structure via vacuum filtration. The PEG molecules were anchored on the GO sheets with hydrogen bonding. Therefore, the resulting PCC exhibited outstanding shape stability with no leakage observed even after several hundred rounds of thermal cycling.

C. Porous material stabilization

PCM stabilization using nanoporous materials has been reported. However, using 3D carbon materials with larger pore scales is much more common. The various methods of shape stabilization facilitated by carbon-based porous materials are discussed in the following section.

3D carbon-based porous materials generally provide shape stability to PCMs through a combination of physical confinement, chemical

bonding, or various forms of intermolecular attraction. Sharing the stabilization mechanisms of microencapsulation and nano-material incorporation, PCCs stabilized with porous carbon materials enjoy the best of both worlds. The abundant types of porous carbon structures provide various options for compositing PCCs depending on the desired functional properties. At the same time, the partial geometric confinement coupled with strong capillary forces allows for a lower leakage rate than achieved by binding interactions alone.

A wide variety of fabrication techniques are employed for the fabrication of these porous carbon-based structures. Directional freezing is a popular and inexpensive method for fabricating porous carbon materials with aligned channel structures.¹²⁸ These channel structures provide excellent shape stability and facilitate PCM crystallization, heat conduction, and compressive strength enhancement.¹²⁹ Therefore, highly thermally conductive, mechanically strong, and shape-stable PCCs with high latent heat can be easily fabricated. Feng *et al.*¹³⁰ provide one of the better examples of PCC stabilization using porous gelatin/nano-graphite aerogels fabricated through directional freezing [see Figs. 10(a) and 10(b)]. The samples can withstand 500 g at 80 °C with minimal shape change and leakage. The solar-thermal energy absorption and conversion efficiency of its composite with PW also reached a high of 92.5%, which proves that thermal energy can be highly effectively transported to and stored throughout the PCC.

Porous carbon-based materials can also be grown onto a metal template using chemical vapor deposition. The metal template can be

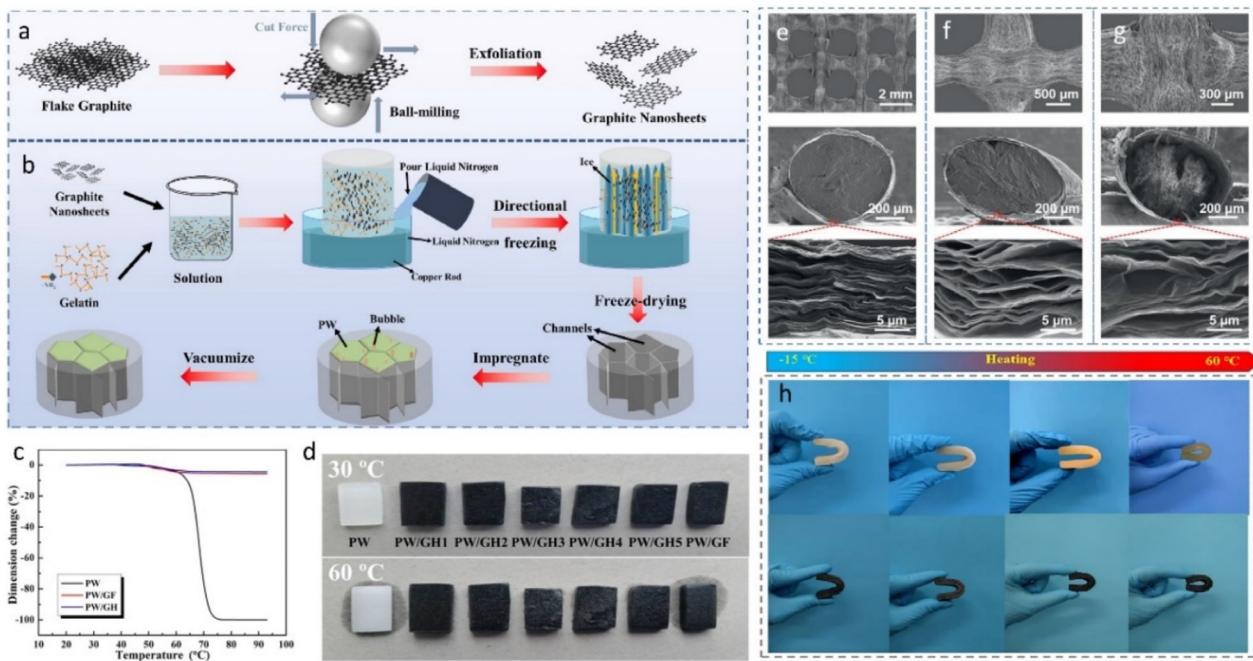


FIG. 10. (a) and (b) Shape stabilization of paraffin/gelatin @ nanographite PCC through the infiltration of PCMs into porous nanographite.¹³⁰ (a) Schematic of the preparation of graphite nanosheets and (b) schematic of the preparation of gelatin @ nanographite aerogel and paraffin/gelatin @ nanographite PCC. Reproduced with permission from Feng *et al.*, Carbon **201**, 756 (2023). Copyright 2023 Elsevier. (c) and (d) Shape stabilization of paraffin/hybrid graphene foam and GA (GH).¹³¹ (c) TMA curves and (d) shape stabilizing effect of pure paraffin, paraffin/graphene foam, and paraffin/GH. Reproduced with permission from Yang, *et al.*, Energy Storage Mater. **13**, 88 (2018). Copyright 2018 Elsevier. (e)–(g) SEM images of bean-pod-structured octadecane (OD)/graphene (BOG) PCCs and their cross sections.¹³² Reproduced with permission from Yang *et al.*, Small **17**(30), 2101093 (2021). Copyright 2021 John Wiley & Sons. (h) Bending test of PA/TPEE/EG samples at various temperatures.¹³⁴ Reproduced with permission from Zhao *et al.*, Chem. Eng. J. **463**, 142514 (2023). Copyright 2023 Elsevier.

etched away, leaving a porous carbon material to be impregnated with PCM. Yang *et al.*¹³¹ applied this method to the fabrication of PW/GH PCCs with excellent shape stability, observing less than 10% dimensional change at a high temperature of $>90^{\circ}\text{C}$ [see Figs. 10(c) and 10(d)].

Another fast-emerging method for fabricating porous graphene-based macrostructures is 3D printing high-concentration GO gels with high viscosities. Yang *et al.*¹³² demonstrated that the leakage of octadecane could be eliminated by simultaneously extruding liquid octadecane into the 3D printed bean-pod-like enclosed porous GO network, as shown in Figs. 10(e)–10(g). No leakage was observed even after 1000 thermal cycles. The large octadecane-free surface and interconnectedness of the GO network show effective solar absorption and high thermal conductivity, therefore enhancing its solar-thermal energy absorption and conversion efficiency to a high of 91%. Sophisticated geometrically shaped PCC samples could also be prepared at a low cost using the GO gel/octadecane simultaneous 3D printing method, opening up new applicational possibilities for these PCCs.

In addition to fabricating 3D porous carbon macrostructures through the assembly of carbon nano-materials, porous carbon-based materials could be directly synthesized from bulk carbon materials. The most scientifically investigated example of these materials is EG. Obtained from the microwave treatment of expandable graphite powders, EGs are inexpensive and easy to produce.¹³³ Despite their low cost, EGs provide excellent shape stability to PCMs like the previously mentioned porous carbon macrostructures. The worm-like morphology of EG determines that it is highly flexible. Zhao *et al.*¹³⁴ demonstrated that a flexible phase-changing filler could be fabricated by mixing paraffin with a thermoplastic polyester elastomer (TPEE). A shape-stable PCC could be obtained by directly mixing EG with liquid paraffin/TPEE. Owing to the synergistic stabilizing effect of the TPEE and EG, the best leak rate of the samples can be controlled to lower than 0.2% after heating at 60°C for 2 h. Meanwhile, the PCC exhibits excellent flexibility, withstanding stretching, twisting, and bending from 15°C to 60°C without fracturing, as shown in Fig. 10(h), filling the previously unoccupied niche of shape stable flexible PCCs, and potentially filling new applicational needs.

VI. APPLICATIONS OF SHAPE-STABLE CARBON-BASED ORGANIC PHASE CHANGE COMPOSITES WITH HIGH LATENT HEAT

Carbon-based materials are primarily composed with organic PCMs to promote efficient charging and discharging due to low density and high thermal conductivity.⁶⁴ Large amounts of research on carbon-based organic PCC in the 2000s and 2010s focused heavily on enhancing thermal conductivity, often overlooking other crucial properties of the PCC.¹⁵ However, with the gradual decrease in the price of carbon-based materials and the dissemination of PCC's wider scope of engineering applications in the latter half of the 2010s and early 2020s, researchers have begun to appreciate the importance of other crucial properties for PCC application. Latent heat and shape stability have gained particular attention, being the determining factors of the PCC's energy storage density and longevity.¹³⁵

The much higher energy storage density of carbon-based organic PCCs has determined that it would gain strongholds in a number of important emerging applications, including solar-thermal energy conversion and storage, thermal management of batteries and electronic

devices, thermal regulating textiles, and infrared (IR) responsive devices for IR remote sensing.

A. Solar-thermal energy conversion and storage

Direct solar-thermal energy conversion is one of the most efficient ways of converting solar energy into energy forms available for direct consumption. Carbon-based materials, such as graphene, CNTs, and metal-organic framework (MOF)-derived carbon, can convert solar energy into heat by delocalizing electrons in the conjugated and hyperconjugated effects.¹³⁶ Then, organic PCMs with large latent heat can absorb the heat generated by the carbon-based materials. Compared to conventional solar-thermal conversion materials, such as metallic nanoparticles and copper sulfide, carbon-based materials have a broader solar absorption spectrum, provide better shape stability for organic PCMs, and are lighter in weight.¹³⁶ Compared to the solar-thermal conversion and storage efficiency of $\sim 40\%$ for pure paraffin, the solar-thermal conversion and storage efficiency of most carbon-based organic PCCs exceeds 80%.^{22,137}

In the last three years, the highest solar-thermal efficiencies have been reported from highly porous graphene and CNT-based PCCs. Sun *et al.*¹³⁸ fabricated a flexible GA-based composite phase change film, reaching 96.0% solar-thermal conversion and storage efficiency at 80.1% PW loading [see Figs. 11(a)–11(e)]. Similarly, Meng *et al.*¹³⁹ vacuum-impregnated a high-density polyethylene foam (HDPE) with PEG, CNTs, and carbon fibers [see Figs. 12(a)–12(c)]. The resulting PCC had a record-high solar-thermal conversion and storage density of 98.1%. In both cases, the carbon-based material formed a highly connected micro-porous thermally conductive network either on its own or using a polymer scaffold. The rough and porous surface of the PCC induces multiple reflections and scattering of the incident light, enhancing its conversion to heat by carbon materials. The heat is conducted throughout the bulk of the PCC via the interconnected network of carbon materials. The network's microscale pores allow PCMs to have sufficient contact surface with the carbon materials, facilitating heat absorption by the PCMs, therefore promoting the solar-thermal conversion and absorption efficiency to over 95% [see Fig. 12(d)].^{22,102,138–149}

Early-stage real applications of lightweight, shape-stable carbon-based organic PCCs with high solar-thermal conversion efficiencies have been made to provide insulation for roofing materials.¹⁵⁰ Under direct sunlight, the roofing PCC absorbs solar energy during the daytime and undergoes fusion. At nighttime, the roofing PCC then undergoes solidification and releases heat. Therefore, the temperature fluctuation under the roof can be controlled.

B. Thermal management of batteries and electronic devices

Temperature control is a key factor in determining the safety of rechargeable batteries, such as lithium batteries. When such batteries are overcharged or internally short-circuited due to impact, heat may accumulate in the batteries. Runaway heat accumulation may lead to fire outbreaks and explosions.¹⁵¹

Due to their high latent heat, high thermal conductivity, shape stability, and compactness, carbon-based organic PCCs are often used alongside rechargeable batteries to prevent these catastrophic events from occurring, particularly during the charging process.¹⁵² The lifespan and performance of many batteries and electronic devices are also

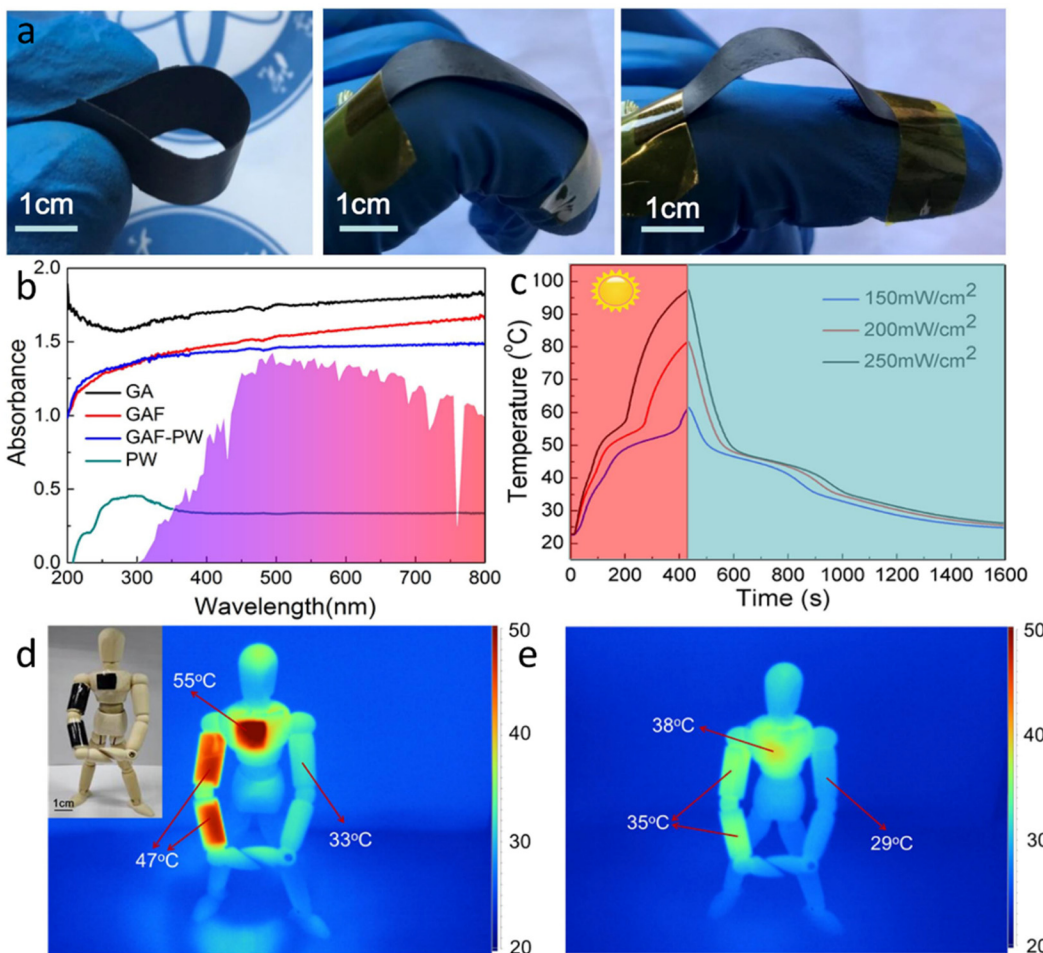


FIG. 11. (a)–(e) GAF-PW (graphene aerogel film-paraffin wax) PCC film for solar-thermoregulation.¹³⁸ (a) Digital images of the flexible GAF-PW PCC film; (b) UV-visible absorption spectrum of PW, GA, GAF, and GAF-PW; (c) Solar-thermal conversion curves of GAF-PW PCC film with different irradiation intensity; IR images of human model with GAF-PW PCC film coated on the one side of arm and chest (d) under the irradiation for 210 s and (e) after removing the irradiation for 10 s. Reproduced with permission from Sun *et al.*, Chem. Eng. J. **419**, 129637 (2021). Copyright 2021 Elsevier.

closely related to their operating temperature. The energy efficiency and lifespan of batteries and other electronic components can be increased by preventing overheating and overcooling. A good example is provided by the PCC by Li *et al.*¹⁵³ in which a highly dense graphene foam is infiltrated with PW, as shown in Fig. 13(a). The PW is contained in the pores of the graphene foam [see Figs. 13(b)–13(g)], which provides much-improved shape stability for the PW [see Figs. 13(h) and 13(i)] as well as a path for thermal conduction. Therefore, after being packaged inside an electronics system, as shown in Fig. 13(j), the PCC can significantly help the electronics system's overheating problem, as shown in Fig. 13(k). The low leakage is particularly interesting for PCC intended for the thermal management of batteries and electronic devices since leaked PCM may also be a risk factor for short-circuiting.¹⁵⁴

C. Thermoregulating textiles

Compared to actively heating and cooling an entire living environment, wearing clothes made out of thermoregulating textiles offers

an environmentally friendly solution for providing thermal comfort to a person. Due to their lightweight, non-toxicity, hydrophobicity, high thermal conductivity, and large latent heat, carbon-based organic PCCs are favorable candidates for fabricating thermoregulating textiles.¹⁵⁵ Due to their simplicity and the vulnerability of organic PCMs to evaporation and thermal degradation during heat treatment, the fabrication of carbon-based organic PCC fibers for thermoregulating textiles has favored direct wet-spinning and 3D printing methods.

Niu *et al.*¹⁵⁶ developed a facile and scalable wet-spinning method for fabricating CNT/polyurethane (PU)/LA PCC fibers using *N,N*-dimethylformamide (DMF) as the solvent, and water as the coagulation bath as shown in Fig. 14(a). During the coagulation process, the rapid diffusion of DMF into the water caused aggregation of the PU chains, LA molecules, and CNTs [See Fig. 14(b)]. Meanwhile, due to their smaller molecular weight, the LA molecules migrated into the fiber's core, while the PU molecules were aligned along the fiber axis direction and remained on the outer layer. As a result, an LA-PU

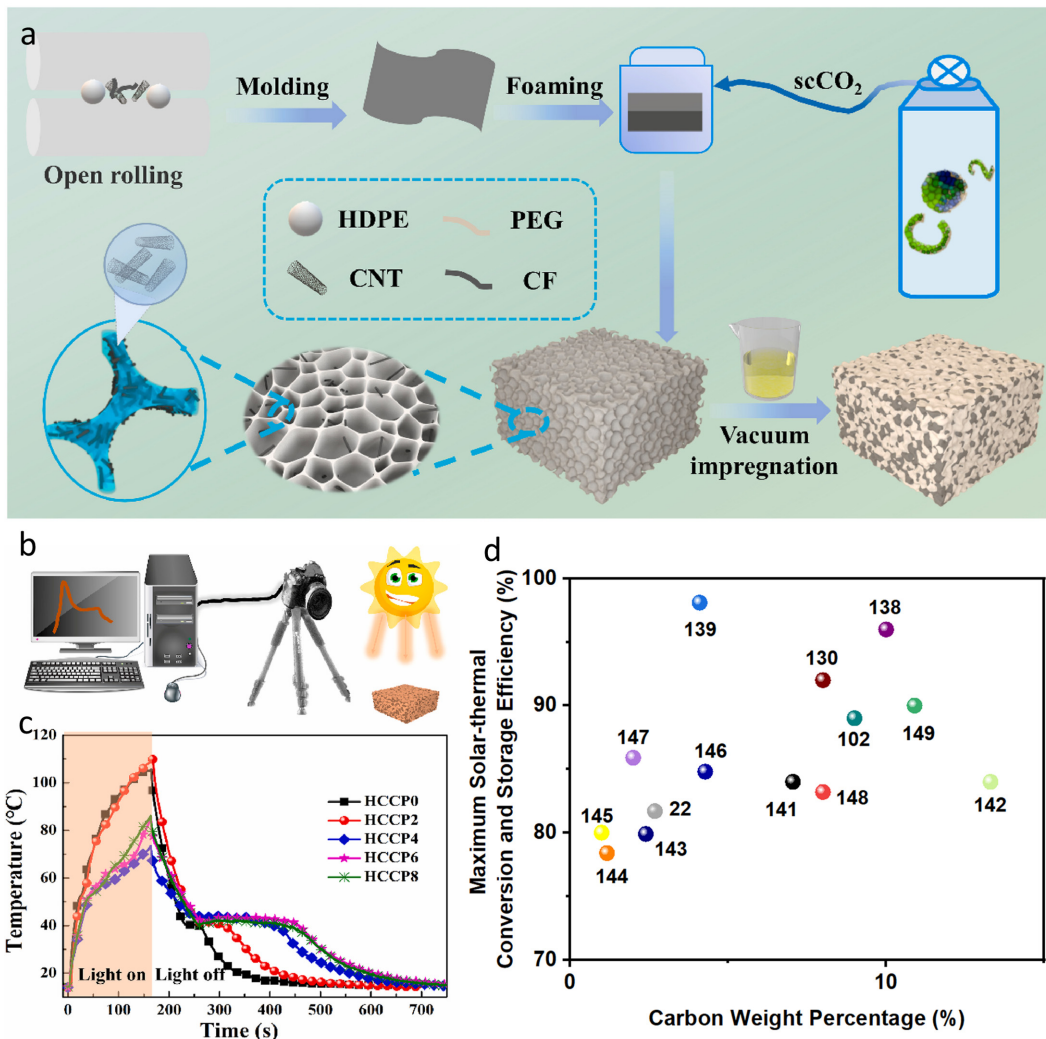


FIG. 12. (a)–(c) HDPE/CNT/CF/PEG PCCs for solar-thermal energy conversion and storage.¹³⁹ (a) Schematic of supercritical CO_2 (sc CO_2)-assisted preparation of HDPE/CNT/CF/PEG PCC; (b) Schematic of solar-thermal conversion testing set up; and (c) Temperature-time of HDPE/CNT/CF/PEG PCC curves during solar-thermal conversion testing. Reproduced with permission from Meng *et al.*, Polymer **271**, 125828 (2023). Copyright 2023 Elsevier.

24 October 2024 08:43:27

core-sheath fiber structure with CNTs dispersed in between was formed. Owing to the alignment of PU, the PCC fiber is highly flexible and can be easily co-woven with cotton fibers into wearable fabrics. Confinement by the PU chains also enhances the crystallization of the LA in the fiber core, enhancing the fibers' latent heat. The well-dispersed CNTs in the PCC fiber do not hinder the crystallization of LA while greatly enhancing the PCC fiber's thermal conductivity, allowing for quick thermal responses as shown in Figs. 14(c) and 14(d) and efficient solar-thermal conversion shown in Fig. 14(e).

Similarly, Yang *et al.*¹⁵⁷ employed CNTs, an organic PCM, and a flexible polymer to fabricate flexible and robust thermoregulating PCC fibers through 3D printing, as shown in Figs. 14(f) and 14(g). In the method of Yang *et al.*, PEG was grafted with thermoplastic polyurethane (TPU) in a DMF solution. The grafted PEG was mixed with

SWCNTs and extruded into a non-woven fabric at 180 °C, and the resulting non-woven fabric is shown in Fig. 14(h). The PCC fibers in the non-woven fabric are highly flexible due to the intertwining PEG-TPU molecular chains. These molecular chains' low surface energy and weak interfacial tension give the non-woven fabric good hydrophobicity. The well-dispersed SWCNTs in each fabric fiber provide high thermal conductivity and fast thermal response, as shown in Figs. 14(i) and 14(j). Compared to wet-spun PCC fabrics, 3D-printed non-woven fabrics save the effort of weaving, thus significantly improving the fabric's output.

D. Infrared-stealth and infrared-responsive materials

Based on the Stefan-Boltzmann law, the two means of achieving IR stealth include reducing a material's IR emissivity and lowering a

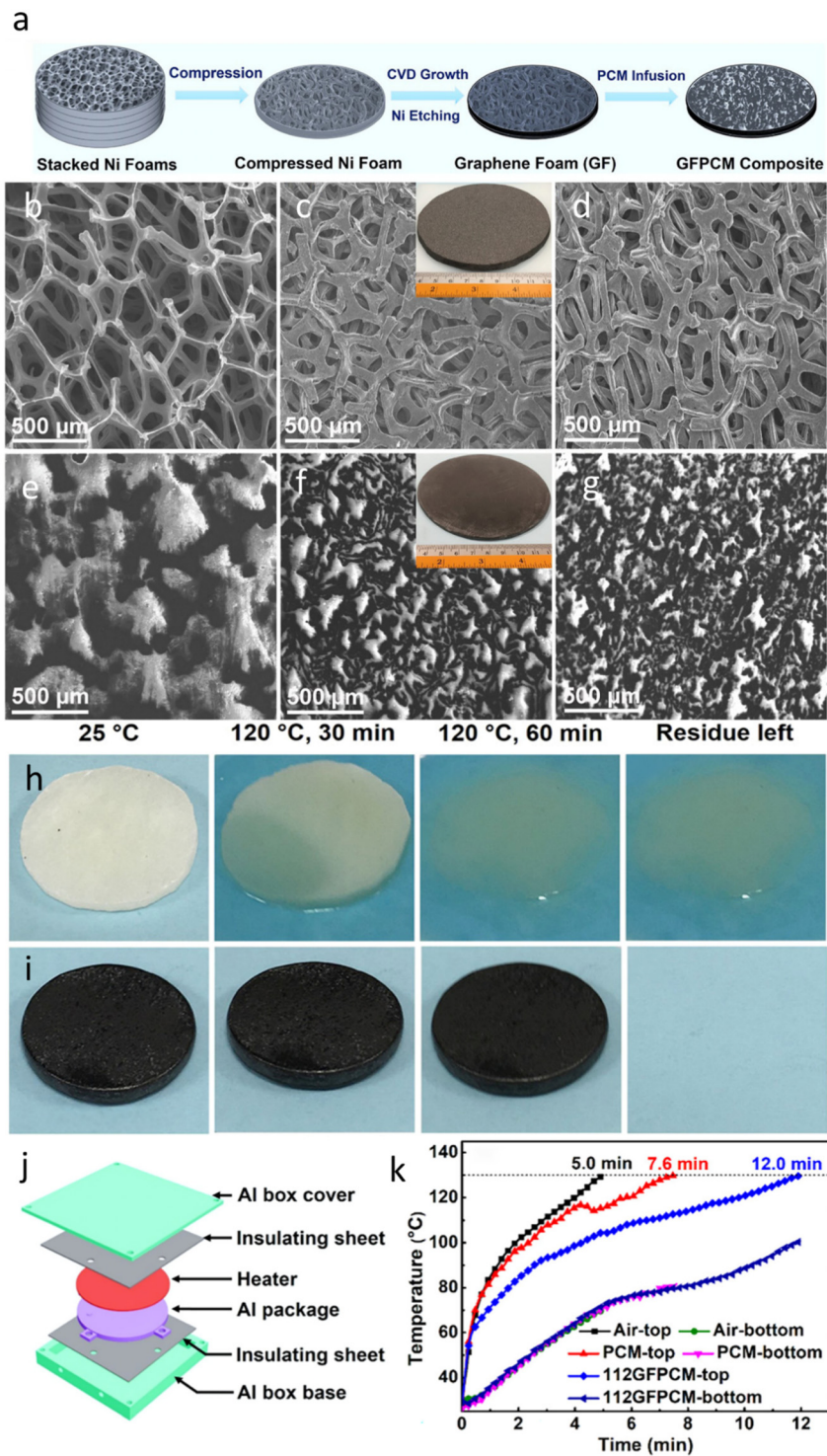


FIG. 13. (a)–(k) Carbon-based organic PCCs for thermal management in electronics:¹⁵³ (a) schematic of the preparation process of graphene foam/PW PCCs; SEM images of (b)–(d) graphene foams with three different densities and (e)–(g) their corresponding PCCs; (h)–(i) Digital photographs of pure PW and graphene foam/PW PCCs at 25 and 120 °C for some time; (j) Illustration of the stack-up assembly of the testing setup for thermal performance evaluation; and (k) Temperature vs time curves of the top and bottom centers of Al packages based on air, pure PW, and graphene foam/PW samples. Reproduced with permission from Li *et al.*, ACS Appl. Nano Mater. 5(6), 8362 (2022). Copyright 2022 American Chemical Society.

material's temperature.¹⁵⁸ Adding IR reflective coating may decrease a material's IR emissivity. However, low IR emitting coatings are often glossy and have high visible reflectiveness, limiting their scope of use.¹⁵⁹ Carbon-based materials have low emissivity in the visible

wavelength. However, they often have high IR emissivity, making them highly detectable to IR cameras under an elevated temperature.¹⁶⁰ Therefore, to limit the visible and IR detectability of the PCC, a layer of organic PCMs is often added underneath a carbon-based

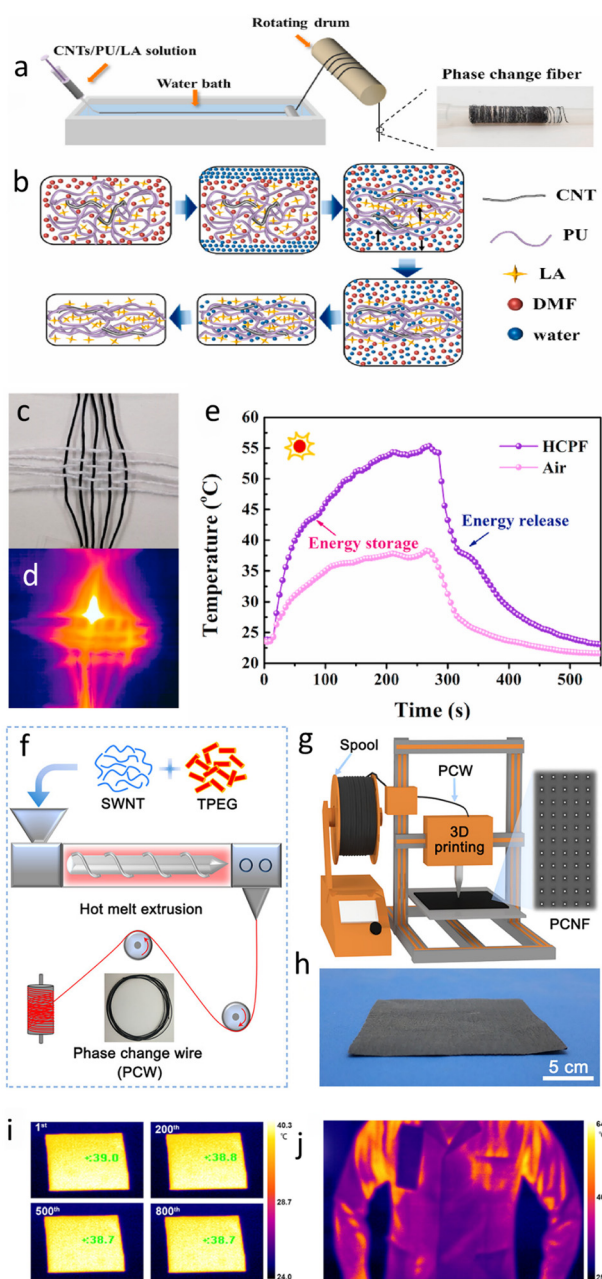


FIG. 14. (a)–(e) CNTs/PU/LA PCC thermoregulating textiles.¹⁵⁶ (a) Schematic of the preparation of the CNTs/PU/LA PCC fiber; (b) mechanism of CNTs/PU/LA PCC fiber formation; (c) CNTs/PU/LA PCC fiber interwoven with cotton fibers; (d) IR image of heated CNTs/PU/LA PCC fiber interwoven with cotton fibers; and (e) temperature-time curves of the CNTs/PU/LA PCC fiber under sunlight radiation. Reproduced with permission from Niu *et al.*, Compos. B Eng. **228**, 109431 (2022). Copyright 2022 Elsevier. (f)–(j) Fabrication procedure and thermal properties of 3D-printed phase change non-woven fabric (PCNF).¹⁵⁷ (f) Melt spinning of phase change wires; (g) 3D printing of PCNF; (h) digital image of a large-scale PCNF; (i) IR images of PCNF after 15 s heating with 800 thermal cycles; and (j) IR image of a person wearing clothes with a PCNF lining. Reproduced with permission from Yang *et al.*, ACS Appl. Mater. Interfaces **14**(5), 7283 (2022). Copyright 2022 American Chemical Society.

material surface to limit the temperature of the carbon-based material and reduce its IR emission [see Figs. 15(a)–15(i)].^{161,162} This IR stealth technology has great potential for military applications, allowing for the protection of personnel and equipment against enemy surveillance.¹⁶³

Due to the π -conjugation effect of heat generation and their low heat capacity, graphene and CNTs' temperature can also rapidly increase in response to IR radiation, making graphene and CNTs excellent IR-responsive materials.^{164,165} Wang *et al.*¹⁶⁶ fabricated a nanocomposite thin film in which 4-methoxyphenyl diazonium functionalized MWCNTs are uniformly distributed in a shape-stable PCM consisting of PEG cross-linked with trifunctional triphenylmethane-triisocyanate (TTI). Under IR radiation, the MWCNTs generate heat quickly. This heat is conducted to the shape-stable PCM. The reversible fusion and solidification of the crystalline PEG in the shape-stable PCM matrix affected the thickness of the interfacial PCM between the functionalized MWCNTs and, therefore, the tunneling efficiency of the electrons between the functionalized MWCNTs. The resulting electrical conductivity of the PCC can be used to sense the presence of IR radiation.

VII. SUMMARY AND OUTLOOK

In this review, we first introduce the basic phase change properties involving PCMs, including phase change temperature, latent heat, solid-liquid phase transition, and supercooling. The thermodynamics of liquid-solid and solid-liquid phase changes are also included to provide a more in-depth understanding of the phase change-related properties of common organic PCMs. With high latent heat, minimal supercooling, and various other favorable attributes, we then focus on organic PCMs and how the carbon-based materials could further enhance their functionality to meet the challenges in modern TES applications. Next, to better understand the evaluation of carbon-based organic PCCs, we dive into common calorimetry methods for characterizing these PCCs. The influence of DSC and the t-history methods on latent heat evaluation is discussed in detail. This helpful insight on the experimental measurement of latent heat allows us to understand the rigorousness needed when evaluating latent heat enhancement efforts. In the past decade, more DSC experiments have shown that the latent heat of carbon-based organic PCCs can be enhanced to exceed that of pure PCMs. Next, we examine the physical and chemical mechanisms that could lead to latent heat enhancement. We group the latent heat enhancement mechanisms into four major categories, including promoting PCM crystallization during solidification, volume expansion control during PCM melting, introducing attractive intermolecular forces between the PCM and carbon-based materials, and forming hydrogen bonds within the PCMs. The particular conditions required for these latent heat enhancement mechanisms are analyzed. The extent to which each mechanism can individually or synergistically enhance latent heat is also discussed, as well as some controversies surrounding the effectiveness of some of the reported latent heat enhancement mechanisms. In addition to latent heat, another essential phase change property of carbon-based organic PCCs is their shape stability. We introduce the various characterization methods for shape stability and discuss the most common methods for enhancing the shape stability of carbon-based organic PCCs, including microencapsulation, nano-material incorporation, and stabilization of PCMs in porous carbon-based materials. The physical and chemical mechanisms of these shape stabilization

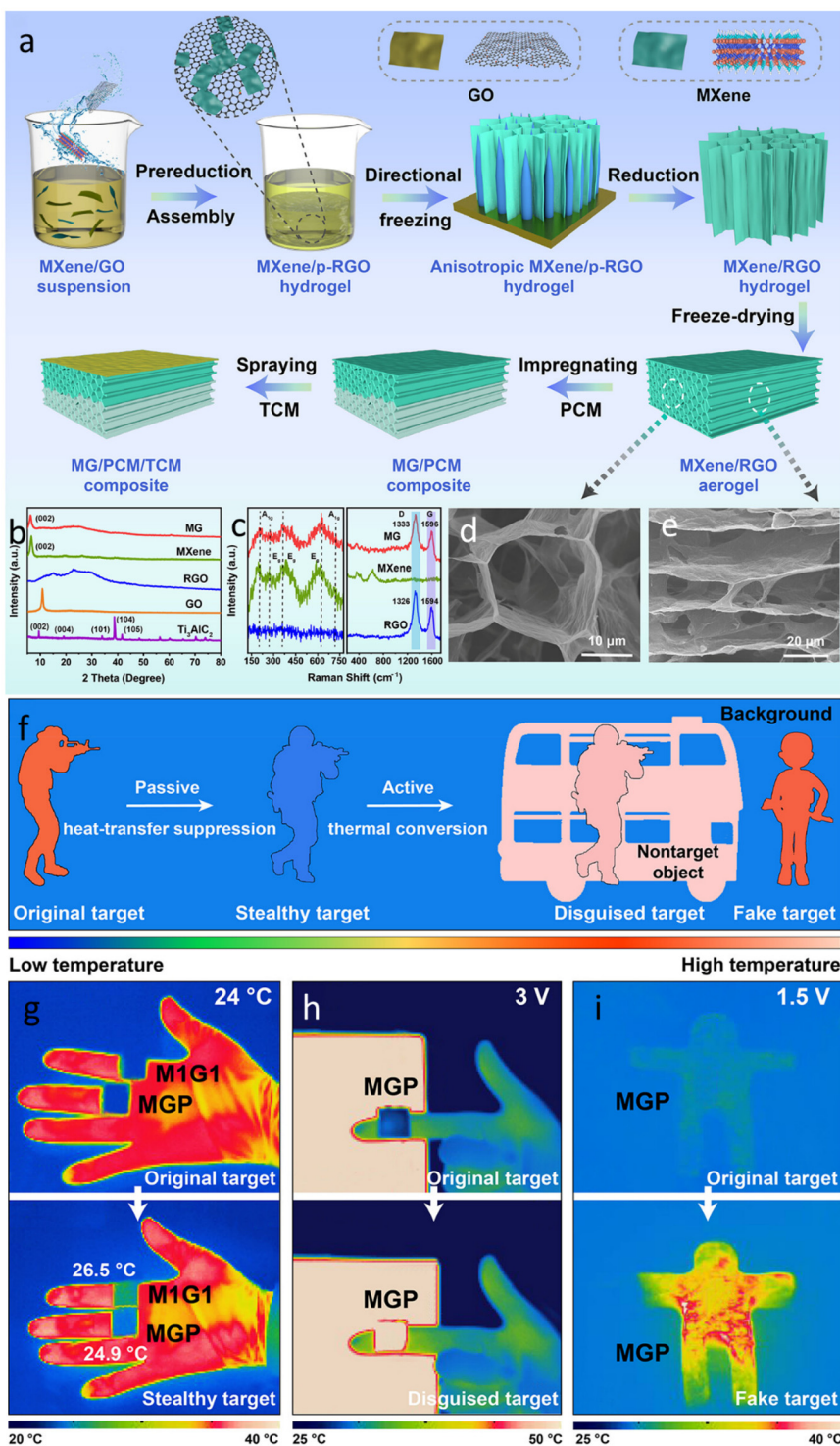


FIG. 15. (a)–(i) rGO-based organic PCCs for IR absorbing applications.¹⁶² (a) Schematic of the preparation of an rGO-based IR absorbing PCC; (b) XRD patterns of the components of the rGO-based PCC; (c) Raman spectra of the components of the rGO-based PCC; (d) and (e) SEM imaged of the rGO-based aerogel; (f) schematic of thermal camouflages in different modes; (g) IR images of the rGO-based aerogel (M1G1) and rGO-based PCC (MGP) covering human fingers; (h) IR camouflage of a low-temperature target in a high-temperature background via electrical heating at 3 V; and (i) IR disguise presentations of the fake target heated by a battery of 1.5 V. Reproduced with permission from Li et al. ACS Nano 17(7), 6875 (2023). Copyright 2023 American Chemical Society.

methods are emphasized. Furthermore, we introduce the latest progress in applying these high latent heat, shape-stable carbon-based organic PCCs. We focus on their applications in solar-thermal energy conversion and storage, thermal management of batteries and other

electronic devices, thermoregulating textiles, and IR stealth and responsive materials.

Research on the development of carbon-based organic PCCs has made considerable strides in the last decade. Many innovative designs

have successfully utilized the favorable thermal properties of these PCCs for the benefit of a wide variety of applications. However, there are still several significant challenges hindering their larger-scale commercial application. The most significant challenge is the high cost of carbon-based materials, such as CNTs, graphene, and MOF-derived carbon.^{136,167} Often more than \$50 per kg, commercially available CNTs, and graphene prices are tens of times higher than that of common organic PCMs such as PW and PEG.^{168–170} Currently, to achieve the desired shape stability, thermal conductivity, and light absorption rate, carbon-based organic PCCs often contain more than 10 wt. % carbon-based materials.^{138,142,171,172} Therefore, instead of the price reduction of carbon-based materials over time, the more feasible approach for cost-effective PCCs is to develop PCCs with lower weight percentages of carbon materials while maintaining the same favorable thermal properties. Less carbon also means that with a higher weight percentage of PCMs, it will be easier for the PCCs to attain high latent heat. Other functional materials could be added to the PCCs without sacrificing too much PCM. These include additives that could enhance the flexibility or hydrophobicity of the PCCs.¹⁷³

Improving the flexibility of carbon-based organic PCCs while retaining their high latent heat, high thermal conductivity, and shape stability is also a significant challenge.¹³⁶ Currently, strategies for fabricating flexible carbon-based organic PCCs most involve using flexible carbon foam, carbon aerogel as a scaffold,^{174,175} or the addition of highly flexible polymers such as PU and melamine foam (MF).^{120,176} Incorporating high weight percentages of carbon foam or carbon aerogel is not a cost-effective approach to overcome the rigidity of organic PCMs. While adding polymers is a much cheaper approach, they reduce the PCC's latent heat and thermal conductivity. When these polymers are added to the PCCs at significant weight ratios, the reduction of latent heat and thermal conductivity becomes a significant problem for the PCC. Therefore, in future research, more efforts should be devoted to optimizing the microstructure of the flexible polymer containing PCCs so better flexibility can be achieved with less polymer. Other options for resolving the conflict between the flexibility and thermal properties of PCCs include the addition of thermally conductive polymers and the introduction of latent heat-enhancing intermolecular forces between the polymers and PCM.¹⁷⁷ More research is needed to study the impact of interactions between polymers and PCMs on the resulting PCCs' latent heat.¹⁷⁸

Standardization efforts should be made for the evaluation methods of the thermal properties of carbon-based organic PCCs, including latent heat, shape stability, and solar-thermal conversion and storage efficiency.¹⁷⁹ The significant discrepancies between existing methods often make the quantitative evaluation of these properties tricky. Standardizing latent heat, shape stability, and solar-thermal conversion and storage efficiency measurement methods will aid in the more rational selection of PCCs for application and help us better identify the potential for improvements in these PCCs.^{180,181}

Finally, further improvements to the thermal properties of carbon-based organic PCCs will be based on a better physical and chemical understanding of the latent heat and shape stability enhancement methods. As we reveal more fundamental physics and chemistry, advanced PCCs with better functional properties and improved thermal and phase change properties can be envisioned to fully realize their practical potential for a broader range of technological applications.

ACKNOWLEDGMENTS

This work was supported by U.S. National Science Foundation under Grant No. DMR 1742806.

AUTHOR DECLARATIONS

Conflict of Interest

The authors have no conflicts to disclose.

Author Contributions

Mingxin Li: Conceptualization (equal); Visualization (lead); Writing—original draft (lead). **Xuanjie Wang:** Conceptualization (equal). **Junhua Shen:** Investigation (equal). **Dong Zhao:** Investigation (equal). **Jie Lian:** Funding acquisition (lead); Supervision (lead); Writing—review & editing (equal).

DATA AVAILABILITY

Data sharing does not apply to this article, as no new data were created or analyzed in this study.

REFERENCES

- ¹P. H. Feng, B. C. Zhao, and R. Z. Wang, *Appl. Therm. Eng.* **166**, 114728 (2020).
- ²G. Alva, Y. Lin, and G. Fang, *Energy* **144**, 341 (2018).
- ³X. Tong, N. Li, M. Zeng, and Q. Wang, *Renewable Sustainable Energy Rev.* **108**, 398 (2019).
- ⁴F. Hassan, F. Jamil, A. Hussain, H. M. Ali, M. M. Janjua, S. Khushnood, M. Farhan, K. Altaf, Z. Said, and C. Li, *Sustainable Energy Technol. Assess.* **49**, 101646 (2022).
- ⁵K. Yuan, J. Shi, W. Aftab, M. Qin, A. Usman, F. Zhou, Y. Lv, S. Gao, and R. Zou, *Adv. Funct. Mater.* **30**(8), 1904228 (2020).
- ⁶A. Allahbaksh and M. Arjmand, *Carbon* **148**, 441 (2019).
- ⁷A.-S. Yang, T.-Y. Cai, L. Su, Y.-S. Li, F.-F. He, Q.-P. Zhang, Y.-L. Zhou, R. He, K. Zhang, and W.-B. Yang, *Sustainable Energy Fuels* **6**(22), 5045 (2022).
- ⁸Z. A. Qureshi, H. M. Ali, and S. Khushnood, *Int. J. Heat Mass Transfer* **127**, 838 (2018).
- ⁹Z. Tao, X. Chen, M. Yang, X. Xu, Y. Sun, Y. Li, J. Wang, and G. Wang, *Sol. Energy Mater. Sol. Cells* **215**, 110600 (2020).
- ¹⁰R. K. Mishra, K. Verma, V. Mishra, and B. Chaudhary, *J. Energy Storage* **50**, 104166 (2022).
- ¹¹C. Amaral, R. Vicente, P. A. A. P. Marques, and A. Barros-Timmons, *Renewable Sustainable Energy Rev.* **79**, 1212 (2017).
- ¹²S. T. Latibari and S. M. Sadrameli, *Sol. Energy* **170**, 1130 (2018).
- ¹³M. Li and J. Lian, *Acc. Mater. Res.* **2**(1), 7 (2021).
- ¹⁴S. Wu, T. Yan, Z. Kuai, and W. Pan, *Energy Storage Mater.* **25**, 251 (2020).
- ¹⁵A. Stonehouse and C. Abeykoon, *Int. J. Heat Mass Transfer* **183**, 122166 (2022).
- ¹⁶B. Eanest Jebasingh and A. Valan Arasu, *Energy Storage Mater.* **24**, 52 (2020).
- ¹⁷X. Chen, Z. Tang, H. Gao, S. Chen, and G. Wang, *iScience* **23**(6), 101208 (2020).
- ¹⁸Y. Liu, Y. Deng, J. Zheng, F. Wu, J. Lu, S. Sun, D. Wu, and T. Wu, *Sol. Energy Mater. Sol. Cells* **248**, 112031 (2022).
- ¹⁹K. Matuszek, R. Vijayaraghavan, M. Kar, and D. R. Macfarlane, *Cryst. Growth Des.* **20**(2), 1285 (2020).
- ²⁰L. Chen, R. Zou, W. Xia, Z. Liu, Y. Shang, J. Zhu, Y. Wang, J. Lin, D. Xia, and A. Cao, *ACS Nano* **6**(12), 10884 (2012).
- ²¹H. Sun, Z. Xu, and C. Gao, *Adv. Mater.* **25**(18), 2554 (2013).
- ²²M. Li, X. Wang, L. Odom, K. Bryce, D. Zhao, J. Shen, Z. Ma, C. Bae, S. Narayan, and J. Lian, *ACS Appl. Mater. Interfaces* **15**(15), 18940 (2023).
- ²³P. Cheng, H. Gao, X. Chen, Y. Chen, M. Han, L. Xing, P. Liu, and G. Wang, *Chem. Eng. J.* **397**, 125330 (2020).

- ²⁴M. A. Almaadeed, S. Labidi, I. Krupa, and M. Karkri, *Thermochim. Acta* **600**, 35 (2015).
- ²⁵Y. Zhang, Z. Jia, A. M. Hai, S. Zhang, and B. Tang, *Composite A* **160**, 107047 (2022).
- ²⁶M. M. Umair, Y. Zhang, K. Iqbal, S. Zhang, and B. Tang, *Appl. Energy* **235**, 846 (2019).
- ²⁷Y. Feng, R. Wei, Z. Huang, X. Zhang, and G. Wang, *Phys. Chem. Chem. Phys.* **20**(11), 7772 (2018).
- ²⁸X. Cao, S. Wu, L. Yang, J. Cui, C. Wang, and A. Li, *Sol. Energy Mater. Sol. Cells* **225**, 111035 (2021).
- ²⁹M. Mehrali, S. Tahan Latibari, M. Mehrali, T. M. I. Mahlia, and H. S. C. Metselaar, *Energy Convers. Manage.* **88**, 206 (2014).
- ³⁰R. Ji, S. Wei, Y. Xia, C. Huang, Y. Huang, H. Zhang, F. Xu, L. Sun, and X. Lin, *J. Energy Storage* **27**, 101134 (2020).
- ³¹B. Tan, Z. Huang, Z. Yin, X. Min, Y. G. Liu, X. Wu, and M. Fang, *RSC Adv.* **6**(19), 15821 (2016).
- ³²F. M. A. Leyva-Gutierrez and T. Wang, *Ind. Eng. Chem. Res.* **60**(41), 14651 (2021).
- ³³D. Milani, M. T. Luu, Y. Li, S. Nelson, and A. Abbas, *Int. J. Greenhouse Gas Control* **115**, 103611 (2022).
- ³⁴K. Dong, N. Sheng, D. Zou, C. Wang, X. Yi, and T. Nomura, *Crystals* **11**(3), 230 (2021).
- ³⁵Y. Shen, S. Liu, A. R. Mazhar, X. Han, L. Yang, and X. E Yang, *Renewable Sustainable Energy Rev.* **141**, 110824 (2021).
- ³⁶Y. Meng, Y. Zhao, Y. Zhang, and B. Tang, *Chem. Eng. J.* **390**, 124618 (2020).
- ³⁷G. T. Nguyen, H. S. Hwang, J. Lee, and I. Park, *ACS Omega* **6**(12), 8469 (2021).
- ³⁸S. Thaker, A. Oluwemi Oni, and A. Kumar, *Energy Convers. Manage.* **153**, 423 (2017).
- ³⁹T. Uchino and C. Fushimi, *Chem. Eng. J.* **419**, 129571 (2021).
- ⁴⁰L. Yang, X. Jin, Y. Zhang, and K. Du, *J. Cleaner Prod.* **287**, 124432 (2021).
- ⁴¹X. Guo, H. Wei, X. He, M. He, and D. Yang, *Build. Environ.* **221**, 109318 (2022).
- ⁴²D. Ghosh, J. Ghose, P. Datta, P. Kumari, and S. Paul, *J. Energy Storage* **53**, 105179 (2022).
- ⁴³A. L. Cottrill, A. T. Liu, Y. Kunai, V. B. Koman, A. Kaplan, S. G. Mahajan, P. Liu, A. R. Toland, and M. S. Strano, *Nat. Commun.* **9**(1), 664 (2018).
- ⁴⁴Y. Zhao, C. Y. Zhao, C. N. Markides, H. Wang, and W. Li, *Appl. Energy* **280**, 115950 (2020).
- ⁴⁵K. A. Thakare and A. Bhave, *Int. J. Eng. Res. Technol.* **4**(10), 176 (2015).
- ⁴⁶R.-A. Mitran, S. Ioniță, D. Lincu, D. Berger, and C. Matei, *Molecules* **26**(1), 241 (2021).
- ⁴⁷P. Papon, J. Leblond, and P. H. Meijer, *The Physics of Phase Transitions: Concepts and Applications* (Springer, 2006).
- ⁴⁸D. Zhang, S. Tian, and D. Xiao, *Sol. Energy* **81**(5), 653 (2007).
- ⁴⁹S. Li and W. H. Thompson, *J. Phys. Chem. B* **109**(11), 4941 (2005).
- ⁵⁰M. P. Allen, *Computational Soft Matter: From Synthetic Polymers to Proteins*, edited by N. Attig, K. Binder, H. Grubmüller, and K. Kremer (John von Neumann Institute for Computing, 2004), Vol. 23, pp. 289–320.
- ⁵¹D. Feng, Y. Feng, Y. Zang, P. Li, and X. Zhang, *Microporous Mesoporous Mater.* **280**, 124 (2019).
- ⁵²K. Y. Leong, S. Hasbi, K. K. Ahmad, N. M. Jali, H. C. Ong, and M. M. Din, *J. Energy Storage* **52**, 105027 (2022).
- ⁵³J. Sun and S. Simon, *Thermochim. Acta* **463**(1-2), 32 (2007).
- ⁵⁴C. L. Jackson and G. B. McKenna, *J. Chem. Phys.* **93**(12), 9002 (1990).
- ⁵⁵Y. Wang, Y. Song, S. Li, T. Zhang, D. Zhang, and P. Guo, *Appl. Clay Sci.* **184**, 105367 (2020).
- ⁵⁶I. Shamseddine, F. Pennec, P. Biwole, and F. Fardoun, *Renewable Sustainable Energy Rev.* **158**, 112172 (2022).
- ⁵⁷M. Thonon, G. Fraisse, L. Zalewski, and M. Pailha, *Appl. Therm. Eng.* **190**, 116751 (2021).
- ⁵⁸M. H. Zahir, S. A. Mohamed, R. Saidur, and F. A. Al-Sulaiman, *Appl. Energy* **240**, 793 (2019).
- ⁵⁹L. Huang, E. Günther, C. Doetsch, and H. Mehling, *Thermochim. Acta* **509**(1), 93 (2010).
- ⁶⁰A. Mollova, R. Androsch, D. Mileva, C. Schick, and A. Benhamida, *Macromolecules* **46**(3), 828 (2013).
- ⁶¹Y.-Q. Wang, S.-S. Lyu, J.-L. Luo, Z.-Y. Luo, Y.-X. Fu, Y. Heng, J.-H. Zhang, and D.-C. Mo, *Appl. Surf. Sci.* **422**, 388 (2017).
- ⁶²T. Wu, N. Xie, J. Niu, J. Luo, X. Gao, Y. Fang, and Z. Zhang, *Int. J. Refrig.* **113**, 136 (2020).
- ⁶³M. Xing, X. Ding, H. Chen, D. Jing, and H. Zhang, *J. Energy Storage* **64**, 107143 (2023).
- ⁶⁴X. Chen, P. Cheng, Z. Tang, X. Xu, H. Gao, and G. Wang, *Adv. Sci.* **8**(9), 2001274 (2021).
- ⁶⁵J. Wang, H. Xie, Z. Xin, Y. Li, and L. Chen, *Sol. Energy* **84**(2), 339 (2010).
- ⁶⁶Z. Ling, J. Chen, T. Xu, X. Fang, X. Gao, and Z. Zhang, *Energy Convers. Manage.* **102**, 202 (2015).
- ⁶⁷H. Mehling, J. Leys, C. Glorieux, and J. Thoen, *SN Appl. Sci.* **3**(202), 1 (2021).
- ⁶⁸H. Fatahi, J. Claverie, and S. Poncet, *Appl. Sci.* **12**(23), 12019 (2022).
- ⁶⁹L. Theresa and R. Velraj, *Mater. Res. Express* **6**(12), 125527 (2019).
- ⁷⁰S. Höhlein, A. König-Haagen, and D. Brüggemann, *Materials* **10**(4), 444 (2017).
- ⁷¹J. Leys, B. Duponchel, S. Longuemart, C. Glorieux, and J. Thoen, *Mater. Renew. Sust. Ener.* **5**(4), 1 (2016).
- ⁷²P. Rolka, T. Przybylinski, R. Kwidzinski, and M. Lackowski, *Renewable Energy* **172**, 541 (2021).
- ⁷³H. Mehling and L. F. Cabeza, *Heat and Cold Storage with PCM* (Springer-Verlag, Berlin, 2008), pp.11.
- ⁷⁴G. W. H. Höhne, W. Hemminger, and H.-J. Flammersheim, *Differential Scanning Calorimetry* (Springer, 2003).
- ⁷⁵ASTM International, *Standard Test Method for Enthalpies of Fusion and Crystallization by Differential Scanning Calorimetry* (ASTM International, USA, 2006), pp. 793-06.
- ⁷⁶H. Selvnes, Y. Allouche, R. I. Manescu, and A. Hafner, *Therm. Sci. Eng. Prog.* **22**, 100807 (2021).
- ⁷⁷S. P. Green, K. M. Wheelhouse, A. D. Payne, J. P. Hallett, P. W. Miller, and J. A. Bull, *Angew. Chem. Int. Ed.* **59**(37), 15798 (2020).
- ⁷⁸L. Li, H. Yu, X. Wang, and S. Zheng, *Energy Build.* **130**, 388 (2016).
- ⁷⁹X. Liu, F. Lin, G. Leng, M. Liu, J. Feng, Y. Bai, Z. Guo, Y. Xu, Z. Sun, and Z. Huang, *J. Energy Storage* **73**, 108959 (2023).
- ⁸⁰R. Liu, A. Li, J. Liu, W. Liu, H. Zheng, Q. Du, X. Chen, and C. Dong, *Chem. Eng. J.* **474**, 145814 (2023).
- ⁸¹S. P. Green, A. D. Payne, K. M. Wheelhouse, J. P. Hallett, P. W. Miller, and J. A. Bull, *J. Org. Chem.* **84**(9), 5893 (2019).
- ⁸²A. Lazaro, E. Günther, H. Mehling, S. Hiebler, J. M. Marin, and B. Zalba, *Meas. Sci. Technol.* **17**(8), 2168 (2006).
- ⁸³Y. Zhang, Y. Jiang, and Y. Jiang, *Meas. Sci. Technol.* **10**(3), 201 (1999).
- ⁸⁴C. Rathgeber, L. Miró, L. F. Cabeza, and S. Hiebler, *Thermochim. Acta* **596**, 79 (2014).
- ⁸⁵A. Solé, L. Miró, C. Barreneche, I. Martorell, and L. F. Cabeza, *Renewable Sustainable Energy Rev.* **26**, 425 (2013).
- ⁸⁶L. F. Cabeza, *Heat and Cold Storage with PCM: An up to Date Introduction into Basics and Applications. Heat and Mass Transfer* (Springer, 2008).
- ⁸⁷S. B. Stanković and P. A. Kyriacou, *Appl. Therm. Eng.* **44**, 78 (2012).
- ⁸⁸M. G. De Paola, C. G. Lopresto, N. Arcuri, and V. Calabro, *Meas. Sci. Technol.* **32**(3), 035601 (2020).
- ⁸⁹P. Rolka, R. Kwidzinski, T. Przybylinski, and A. Tomaszewski, *Materials* **14**(23), 7371 (2021).
- ⁹⁰M. Wu, S. Wu, Y. Cai, R. Wang, and T. Li, *Energy Storage Mater.* **42**, 380 (2021).
- ⁹¹X. Shao, S. Yang, L. Fan, and Y. Yuan, *J. Energy Storage* **68**, 107848 (2023).
- ⁹²X. Li, C. Zou, W. Chen, and X. Lei, *Sol. Energy Mater. Sol. Cells* **157**, 572 (2016).
- ⁹³B. Luo, L. Wu, D. Li, Z. Zhang, X. Yu, G. Li, and H. Song, *Carbon* **196**, 146 (2022).
- ⁹⁴C. Wang, W. Dong, A. Li, D. G. Atinifu, G. Wang, and Y. Lu, *Chem. Eng. J.* **428**, 130605 (2022).
- ⁹⁵S. Wu, T. Li, M. Wu, J. Xu, J. Chao, Y. Hu, T. Yan, Q.-Y. Li, and R. Wang, *ACS Appl. Mater. Interfaces* **13**(16), 19200 (2021).
- ⁹⁶J. Wang, Y. Wang, and R. Yang, *Sol. Energy Mater. Sol. Cells* **140**, 439 (2015).
- ⁹⁷C. Yu and Y. S. Song, *Materials* **15**(13), 4541 (2022).
- ⁹⁸D. G. Atinifu, Y. S. Ok, H. W. Kua, and S. Kim, *Appl. Therm. Eng.* **181**, 115960 (2020).
- ⁹⁹C. Li, L. Fu, J. Ouyang, and H. Yang, *Sci. Rep.* **3**(1908), 1 (2013).
- ¹⁰⁰J. Qiu, X. Fan, Y. Shi, S. Zhang, X. Jin, W. Wang, and B. Tang, *J. Mater. Chem. A* **7**(37), 21371 (2019).

- ¹⁰¹J. F. Li, W. Lu, Y. B. Zeng, and Z. P. Luo, *Sol. Energy Mater. Sol. Cells* **128**, 48 (2014).
- ¹⁰²J. Yang, G.-Q. Qi, Y. Liu, R.-Y. Bao, Z.-Y. Liu, W. Yang, B.-H. Xie, and M.-B. Yang, *Carbon* **100**, 693 (2016).
- ¹⁰³R. J. Warzoha and A. S. Fleischer, *Int. J. Heat Mass Transfer* **79**, 314 (2014).
- ¹⁰⁴R. A. Barnard and A. J. Matzger, *Langmuir* **30**(25), 7388 (2014).
- ¹⁰⁵C. Dong, A. Li, C. Wang, J. Li, H. Gao, X. Chen, Y. Wang, L. Li, Y. Zheng, and G. Wang, *Chem. Eng. J.* **430**, 133007 (2022).
- ¹⁰⁶H. Gao, J. Wang, X. Chen, G. Wang, X. Huang, A. Li, and W. Dong, *Nano Energy* **53**, 769 (2018).
- ¹⁰⁷M. Wang, T. Zhang, D. Mao, Y. Yao, X. Zeng, L. Ren, Q. Cai, S. Mateti, L. H. Li, X. Zeng, G. Du, R. Sun, Y. Chen, J.-B. Xu, and C.-P. Wong, *ACS Nano* **13**(7), 7402 (2019).
- ¹⁰⁸L. Xia, P. Zhang, and R. Z. Wang, *Carbon* **48**(9), 2538 (2010).
- ¹⁰⁹S. Shaikh, K. Lafdi, and K. Hallinan, *J. Appl. Phys.* **103**(9), 094302 (2008).
- ¹¹⁰J. N. Israelachvili, *Intermolecular and Surface Forces* (Elsevier Science, 2011).
- ¹¹¹J. Wang, H. Xie, and Z. Xin, *Thermochim. Acta* **488**(1), 39 (2009).
- ¹¹²X. Zhu, L. Han, Y. Lu, F. Wei, and X. Jia, *Appl. Energy* **254**, 113688 (2019).
- ¹¹³J. Wang, X. Jia, D. G. Atinafu, M. Wang, G. Wang, and Y. Lu, *J. Mater. Chem. A* **5**(46), 24321 (2017).
- ¹¹⁴W. Luo, Y. Feng, C. Qin, M. Li, S. Li, C. Cao, P. Long, E. Liu, W. Hu, K. Yoshino, and W. Feng, *Nanoscale* **7**(39), 16214 (2015).
- ¹¹⁵X. Tan, H. Nian, J. Li, Y. Zhou, F. Zhu, and X. Li, *Energy Fuels* **35**(18), 15126 (2021).
- ¹¹⁶R. Narasimman, S. Vijayan, and K. Prabhakaran, *J. Mater. Sci.* **50**(24), 8018 (2015).
- ¹¹⁷J. Yang, X. Li, S. Han, Y. Zhang, P. Min, N. Koratkar, and Z.-Z. Yu, *J. Mater. Chem. A* **4**(46), 18067 (2016).
- ¹¹⁸X.-H. Wu, Y.-N. Chen, J.-W. Hou, Z.-J. Chang, K. Wang, C. Lv, and H. Liu, *Appl. Therm. Eng.* **212**, 118632 (2022).
- ¹¹⁹S. Sinha-Ray, R. P. Sahu, and A. L. Yarin, *Soft Matter* **7**(19), 8823 (2011).
- ¹²⁰W. Aftab, A. Mahmood, W. Guo, M. Yousaf, H. Tabassum, X. Huang, Z. Liang, A. Cao, and R. Zou, *Energy Storage Mater.* **20**, 401 (2019).
- ¹²¹L. Han, X. Jia, Z. Li, Z. Yang, G. Wang, and G. Ning, *Ind. Eng. Chem. Res.* **57**(39), 13026 (2018).
- ¹²²J. Kim, J. Lee, C. Song, J. Yun, and W. Choi, *Energy Convers. Manage.* **266**, 115853 (2022).
- ¹²³J. Ge, Y. Wang, H. Wang, H. Mao, J. Li, and H. Shi, *Sol. Energy Mater. Sol. Cells* **208**, 110388 (2020).
- ¹²⁴Y. Wu, J. Zhu, and L. Huang, *Carbon* **143**, 610 (2019).
- ¹²⁵S. Zhang, Q. Tao, Z. Wang, and Z. Zhang, *J. Mater. Chem.* **22**(38), 20166 (2012).
- ¹²⁶L. Liu, L. Kong, H. Wang, R. Niu, and H. Shi, *Sol. Energy Mater. Sol. Cells* **149**, 40 (2016).
- ¹²⁷H.-B. Liu, D.-F. Pei, S. Chen, R.-R. Cao, and X.-X. Zhang, *Thermochim. Acta* **661**, 166 (2018).
- ¹²⁸G. Shao, D. A. H. Hanaor, X. Shen, and A. Gurlo, *Adv. Mater.* **32**(17), 1907176 (2020).
- ¹²⁹D. Wang, X. Wu, G. Owens, and H. Xu, *Chin. J. Struct. Chem.* **42**(4), 100006 (2023).
- ¹³⁰J. Feng, X. Liu, F. Lin, S. Duan, K. Zeng, Y. Bai, X. Wu, Z. Huang, and X. Min, *Carbon* **201**, 756 (2023).
- ¹³¹J. Yang, G.-Q. Qi, R.-Y. Bao, K. Yi, M. Li, L. Peng, Z. Cai, M.-B. Yang, D. Wei, and W. Yang, *Energy Storage Mater.* **13**, 88 (2018).
- ¹³²Z. Yang, S. Jia, Y. Niu, X. Lv, H. Fu, Y. Zhang, D. Liu, B. Wang, and Q. Li, *Small* **17**(30), 2101093 (2021).
- ¹³³Q. Wei, L. Xu, Z. Tang, Z. Xu, C. Xie, L. Guo, and W. Li, *J. Ind. Eng. Chem.* **122**, 562 (2023).
- ¹³⁴X. Zhao, K. Lei, S. Wang, B. Wang, L. Huang, and D. Zou, *Chem. Eng. J.* **463**, 142514 (2023).
- ¹³⁵V. V. Tyagi, K. Chopra, R. K. Sharma, A. K. Pandey, S. K. Tyagi, M. S. Ahmad, A. Sari, and R. Kothari, *Sol. Energy Mater. Sol. Cells* **234**, 111392 (2022).
- ¹³⁶G. Wang, Z. Tang, Y. Gao, P. Liu, Y. Li, A. Li, and X. Chen, *Chem. Rev.* **123**(11), 6953 (2023).
- ¹³⁷M. Chen, Y. He, Q. Ye, Z. Zhang, and Y. Hu, *Int. J. Heat Mass Transfer* **130**, 1133 (2019).
- ¹³⁸K. Sun, H. Dong, Y. Kou, H. Yang, H. Liu, Y. Li, and Q. Shi, *Chem. Eng. J.* **419**, 129637 (2021).
- ¹³⁹C. Meng, X. Li, Z. Liu, M. Wang, Y. Chen, Y. Sheng, Z. Liu, Y. Xu, L. Jia, L. Wu, X. Chen, Y. Li, H. Wu, and X. Lu, *Polymer* **271**, 125828 (2023).
- ¹⁴⁰Y. Zhang, J. Wang, J. Qiu, X. Jin, M. M. Umair, R. Lu, S. Zhang, and B. Tang, *Appl. Energy* **237**, 83 (2019).
- ¹⁴¹H.-Y. Zhao, C. Shu, P. Min, C. Li, W. Deng, J. Yang, X. Li, and Z.-Z. Yu, *J. Mater. Chem. A* **10**(42), 22488 (2022).
- ¹⁴²P. Liu, F. An, X. Lu, X. Li, P. Min, C. Shu, W. Li, and Z.-Z. Yu, *Compos. Sci. Technol.* **201**, 108492 (2021).
- ¹⁴³X. Tang, L. Luo, Y. Guo, Z. Yang, K. Zhang, R. He, J. Fan, and W. Yang, *Fullerene Nanotubes Carbon Nanostruct.* **27**(5), 375 (2019).
- ¹⁴⁴Y. Zhou, X. Wang, X. Liu, D. Sheng, F. Ji, L. Dong, S. Xu, H. Wu, and Y. Yang, *Carbon* **142**, 558 (2019).
- ¹⁴⁵L. Zhang, R. Li, B. Tang, and P. Wang, *Nanoscale* **8**(30), 14600 (2016).
- ¹⁴⁶Y. Qian, N. Han, Z. Zhang, R. Cao, L. Tan, W. Li, and X. Zhang, *ACS Appl. Mater. Interfaces* **11**(49), 45832 (2019).
- ¹⁴⁷D. Hu, L. Han, W. Zhou, P. Li, Y. Huang, Z. Yang, and X. Jia, *Chem. Eng. J.* **437**, 135056 (2022).
- ¹⁴⁸Y. Sun, N. Zhang, Q. Sun, X. Cao, X. Shao, and Y. Yuan, *J. Energy Storage* **63**, 107043 (2023).
- ¹⁴⁹Z. Tao, H. Zou, M. Li, S. Ren, J. Xu, J. Lin, M. Yang, Y. Feng, and G. Wang, *J. Colloid Interface Sci.* **629**, 632 (2023).
- ¹⁵⁰S. Xi, L. Wang, H. Xie, and W. Yu, *Int. J. Hydrogen Energy* **47**(23), 12024 (2022).
- ¹⁵¹L. Bravo Diaz, X. He, Z. Hu, F. Restuccia, M. Marinescu, J. V. Barreras, Y. Patel, G. Offer, and G. Rein, *J. Electrochem. Soc.* **167**(9), 090559 (2020).
- ¹⁵²S. Wilke, B. Schweitzer, S. Khateeb, and S. Al-Hallaj, *J. Power Sources* **340**, 51 (2017).
- ¹⁵³H. Li, R. Y. Tay, S. H. Tsang, R. Hubert, P. Coquet, T. Merlet, J. Foncin, J. J. Yu, and E. H. T. Teo, *ACS Appl. Nano Mater.* **5**(6), 8362 (2022).
- ¹⁵⁴S. Wang, K. Lei, Z. Wang, H. Wang, and D. Zou, *Chem. Eng. J.* **438**, 135559 (2022).
- ¹⁵⁵B. Mu and M. Li, *Sci. Rep.* **8**(1), 8878 (2018).
- ¹⁵⁶Z. Niu, S. Qi, S. S. A. Shuaib, and W. Yuan, *Compos. B Eng.* **228**, 109431 (2022).
- ¹⁵⁷Z. Yang, Y. Ma, S. Jia, C. Zhang, P. Li, Y. Zhang, and Q. Li, *ACS Appl. Mater. Interfaces* **14**(5), 7283 (2022).
- ¹⁵⁸R. Xu, W. Wang, and D. Yu, *Compos. Struct.* **212**, 58 (2019).
- ¹⁵⁹K. Wang, C. Wang, Y. Yin, and K. Chen, *J. Alloys Compd.* **690**, 741 (2017).
- ¹⁶⁰M. C. Larciprete, S. Paoloni, N. Orazi, F. Mercuri, M. Orth, Y. Gloy, M. Centini, R. Li Voti, and C. Sibilia, *Int. J. Therm. Sci.* **146**, 106109 (2019).
- ¹⁶¹T. Shi, Z. Zheng, H. Liu, D. Wu, and X. Wang, *Nanomaterials* **11**(11), 3038 (2021).
- ¹⁶²B.-X. Li, Z. Luo, W.-G. Yang, H. Sun, Y. Ding, Z.-Z. Yu, and D. Yang, *ACS Nano* **17**(7), 6875 (2023).
- ¹⁶³J. Hu, Y. Hu, Y. Ye, and R. Shen, *Chem. Eng. J.* **452**, 139147 (2023).
- ¹⁶⁴M. Mazurkiewicz-Pawlacka, M. Nowak, A. Malolepszy, A. Witowski, D. Wasik, Y. Hu, and L. Stobinski, *Nanomaterials* **10**(1), 32 (2019).
- ¹⁶⁵X. He, F. Léonard, and J. Kono, *Adv. Opt. Mater.* **3**(8), 989 (2015).
- ¹⁶⁶Y. Wang, H. Mi, Q. Zheng, Z. Ma, and S. Gong, *ACS Appl. Mater. Interfaces* **7**(38), 21602 (2015).
- ¹⁶⁷R. Yang, X. Guo, H. Wu, W. Kang, K. Song, Y. Li, X. Huang, and G. Wang, *Biochar* **4**(1), 38 (2022).
- ¹⁶⁸S. Xu, J. Zhou, J. Wang, S. Pathiranage, N. Oncel, P. R. Ilango, X. Zhang, M. Mann, and X. Hou, *Adv. Funct. Mater.* **31**(32), 2101645 (2021).
- ¹⁶⁹J. Han, J. S. Chae, J. C. Kim, and K. C. Roh, *Carbon* **163**, 402 (2020).
- ¹⁷⁰A. H. Ali, S. I. Ibrahim, Q. A. Jawad, R. S. Jawad, and M. T. Chaichan, *Case Stud. Therm. Eng.* **15**, 100537 (2019).
- ¹⁷¹D. Yan, W. Ming, S. Liu, G. Yin, Y. Zhang, B. Tang, and S. Zhang, *J. Energy Storage* **36**, 102428 (2021).
- ¹⁷²M. Maleki, P. T. Ahmadi, H. Mohammadi, H. Karimian, R. Ahmadi, and H. B. M. Emrooz, *Sol. Energy Mater. Sol. Cells* **191**, 266 (2019).
- ¹⁷³G. Li, G. Hong, D. Dong, W. Song, and X. Zhang, *Adv. Mater.* **30**(30), 1801754 (2018).
- ¹⁷⁴J. Shi, M. Qin, W. Aftab, and R. Zou, *Energy Storage Mater.* **41**, 321 (2021).
- ¹⁷⁵P. Cheng, Z. Tang, Y. Gao, P. Liu, C. Liu, and X. Chen, *iScience* **25**(5), 104226 (2022).

- ¹⁷⁶Y.-Y. Xiao, D.-Y. Bai, Z.-P. Xie, Z.-Y. Yang, J.-H. Yang, X.-D. Qi, and Y. Wang, *Compos. A* **146**, 106420 (2021).
- ¹⁷⁷S. Y. Pak, H. M. Kim, S. Y. Kim, and J. R. Youn, *Carbon* **50**(13), 4830 (2012).
- ¹⁷⁸A. Fallahi, G. Guldenlops, M. Tao, S. Granados-Focil, and S. Van Dessel, *Appl. Therm. Eng.* **127**, 1427 (2017).
- ¹⁷⁹R. K. Sharma, P. Ganesan, V. V. Tyagi, H. S. C. Metselaar, and S. C. Sandaran, *Energy Convers. Manage.* **95**, 193 (2015).
- ¹⁸⁰W. Aftab, A. Usman, J. Shi, K. Yuan, M. Qin, and R. Zou, *Energy Environ. Sci.* **14**(8), 4268 (2021).
- ¹⁸¹C. Barreneche, H. Navarro, S. Serrano, L. F. Cabeza, and A. I. Fernández, *Energy Procedia* **57**, 2408 (2014).